

Received January 25, 2022, accepted February 8, 2022, date of publication February 16, 2022, date of current version March 3, 2022.

Digital Object Identifier 10.1109/ACCESS.2022.3152190

Fault-Tolerant Control for AUVs Using a Single Thruster

DICTINO CHAOS^{ID}, DAVID MORENO-SALINAS^{ID}, AND JOAQUÍN ARANDA

Department of Computer Science and Automatic Control, National Distance Education University (UNED), 28040 Madrid, Spain

Corresponding author: David Moreno-Salinas (dmoreno@dia.uned.es)

This work was supported in part by Ministerio de Ciencia e Innovación of Spain under Reference PID2020-112502RB-C44, and in part by Universidad Nacional de Educacion a Distancia (UNED) under Reference 096-034095.

ABSTRACT The present paper presents a fault-tolerant control for an AUV in the presence of a critical failure in the actuators that may require an emergency operation to recover it or to drive it to a safe point. In this context, the control scheme proposed deals with a single thruster in operational conditions to command the vehicle towards a desired direction and reach a safe target point. In addition, the AUV is commanded with only two control actions on the available thruster, driving the vehicle through the desired direction following a spiral-like path and keeping it within the neighbourhood of the target point. The fault-tolerant control proposed is simple and robust enough to be applied to multiple kinds of AUVs without the need of accurate parameter design. The stability and well performance of the control scheme proposed is analytically demonstrated, and simulation examples illustrate the key results derived.

INDEX TERMS AUV, critical failure, emergency operations, fault-tolerant control.

I. INTRODUCTION

Oceans cover approximately 70% of Earth's surface and represent the largest reservoir of life and resources. The interest in investigating, exploring and exploiting the ocean resources and the preservation of the marine life and environment has been increasing over the last years, and many efforts are being undertaken in this area to develop efficient and reliable tools.

In recent years, the use of Autonomous Underwater Vehicles (AUVs) is increasing significantly and they are becoming ubiquitous in multiple commercial and research operations at sea, due to their reliability and relative low cost. In addition, their flexibility, adaptability and autonomy make them a powerful tool to replace remotely operated vehicles (ROVs) and also humans in the execution of many demanding tasks at sea. The latter include offshore inspection, pipeline inspection, ocean exploration, habitat mapping, archaeological site mapping, localization and tracking of underwater targets, etc. Furthermore, their use in collaborative tasks allows for the realization of complex missions, often with relatively simple systems, see for example [1]–[3] and the references therein.

Many AUV missions are carried out on harsh environments and involve critical systems, so the behaviour of the AUVs

The associate editor coordinating the review of this manuscript and approving it for publication was Shihong Ding^{ID}.

must be reliable and efficient, and they must work correctly for extended time. However, in practical applications, the malfunction or failure of any or some of the AUV systems and actuators is common. A failure on the AUV may result in the loss of the vehicle, and even put environment, or human and animal lives at risk. Therefore, a fault-tolerant system becomes essential to keep the control of the vehicle and recover it in case of critical failure.

A fault-tolerant system is composed of three modules: fault detection, fault isolation and fault accommodation [4]. Fault detection deals with the problem of recognising that there is a failure in the vehicle that prevents it from a correct operation. Fault isolation deals with the identification of the cause of the failure and its location. Finally, fault accommodation is concerned with the control of the vehicle to execute a desired task in the presence of failure. Fault detection and isolation have been extensively studied, the reader is referred to [5] and the references therein. In this work we will focus on the third module, fault accommodation, to develop a fault-tolerant control strategy for the AUV motion execution in case of critical thruster failure.

We can find multiple solutions and approaches about fault-tolerant diagnosis and control of AUVs in literature. For example, in [4] and [6] the authors investigate fault-tolerant control schemes for an AUV with thruster redundancy.

In these works, the existence of redundant thrusters is exploited to overcome failures during operation by thruster force allocation of the remaining actuators. In [7] the authors deal with the dynamic modelling of the propulsion system of an AUV together with a fault-tolerant control by reallocating thruster control forces. In [8] a reconfigurable layout for an inspection vehicle is developed. This layout is based on four pivoted thrusters than can be configured depending on the requirements and mission, and provides robustness in case of failure of one of the thrusters. In [9] a dynamic surface fault-tolerant control for ROVs is presented for trajectory tracking operations. The vehicle considered is fully-actuated, and a fault-tolerant thruster allocation policy is used in order to distribute the moments and forces among the remaining thrusters, showing good performance for tracking operations.

The above works consider the existence of multiple thrusters and actuators that can compensate the failure of one of them by reallocating and reconfiguring the forces provided by the remaining thrusters.

Other works study the situation in which the thruster failure reduces the number of degrees of freedom (DOF) of the vehicle. For example, in [10] geometric control theory is used to design trajectories to recover an AUV after an actuator failure. For this purpose the AUV is modelled as a forced affine connection control system, and the control is carried out using integral curves of rank one and kinematic reductions. In this case, the actuator failure implies a reduction of the available DOF, making the vehicle underactuated. In [11] a method for computing online the controller of an AUV under thruster failures is proposed. To this end, an optimization problem on a specific class of functions is defined to compute an optimal control law without using the faulty thruster. This work is extended in [12] where an online learning-based method to discover control policies to overcome thruster failures is proposed. The method is applied to a fully-actuated vehicle, which may become underactuated after the failure of one of the thrusters. For this purpose, a linear function approximator is considered to represent the fault-tolerant policy, whose parameters are learned depending on the AUV model and the mission. The AUV model is learned on board, and then it is adapted when a failure occurs. In [13] a fault-tolerant control for underactuated vehicles is developed by using a composite neural learning fault-tolerant control for path following, considering event-triggered input. The actuator faults considered are partial loss of effectiveness and bias fault, both for the rudder servo and the main engine of the vehicle, and the control scheme is able to compensate the actuator failures.

In addition, fault-tolerant control may be applied to many different kinds of vehicles and systems, see for example [14], [15] or [16]. In [14] the fault-tolerant control of a free-swimming robotic fish is studied, which is based on a feedback controller and a feed-forward compensator. In [15] the authors developed a robust fault-tolerant H_∞ control with adaptive compensation. A dynamic output feedback controller, which guarantees the stability and adaptive H_∞

performance of the closed loop system, is designed by stabilizing controller gains and adaptive control gain functions, and it is applied to a linearized dynamic aircraft system. In [16] a quantized non-fragile feedback control problem for active suspension systems with and without actuator faults is studied, where ride comfort, road holding ability and hard constraints on suspension deflection and actuator are considered in a multi-objective control problem.

It is important to notice that for an adequate fault-tolerant control, the identification and isolation of the problem is imperative. In this sense, we can find some works that deal with the complete system, such as [17], where an observer-based fault diagnosis approach is studied to detect, isolate and identify actuator faults of an AUV, where SVM is used to compensate the unmodelled dynamics. In [18], the authors propose an actuator fault-tolerant control scheme, which is composed of detection, isolation and accommodation of fault modules, and a sliding mode approach is used for the vehicle control and fault isolation. The vehicle configuration shows redundancy of actuators, which is exploited to deal with the failure and continue with the mission objectives. In [19] an algorithm based on a Bayesian Filter that detects failures in thrusters in run-time is developed. This algorithm adapts the vehicle's dynamical model to take into account the faulty thruster. The approach is applied to a fully-actuated vehicle where one of the thrusters has a malfunction. In [20] a finite-time fault-tolerant trajectory control using integral sliding mode manifold is developed. In addition, a fault-estimator is designed to detect, isolate and accommodate unknown faults and disturbances in a 3-DOF fully-actuated autonomous surface vehicle (ASV) model.

Other interesting approaches are [21], where a fault-tolerant lateral control against actuator faults is developed using a Kalman Filter for identification of the control distribution matrix and a linear quadratic regulator (LQR) is used for the controller; [22] where an intelligent monitoring and emergency system is developed based on an ontological approach, which consists of three blocks, one for the formation of knowledge on fault diagnosis, a translator to convert knowledge in code, and the emergency system; and [23], where an adaptive fault-tolerant control method based on virtual closed-loop system and an improved second-order sliding mode observer are developed and tested for an overactuated vehicle. In [24] an adaptive sliding model fault-tolerant fuzzy tracking control is developed. A Takagi-Sugeno fuzzy model is considered. This strategy tries to ensure the accessibility of the sliding motion in case of actuators faults, being able to deal with 2 simultaneous actuators faults considering a fully-actuated marine vehicle. Reference [25] also considers a Takagi-Sugeno fuzzy model for designing a fault-tolerant control for dynamic positioning, where quantized feedback sliding model control is used. In [26] a fault-diagnosis observer and a fault-tolerant control are designed for ASVs in network environments. Fault-tolerant control is based on the observer to compensate the actuators faults. A sliding mode fault-tolerant control with signal quantization

is described in the presence of time-delay and various thruster faults in [27], and in [28] a fault-tolerant control using integral sliding mode output feedback is used for compensating for thruster faults and disturbances, where thruster redundancy is assumed to fully compensate for stuck fault. For a deeper review on fault-tolerant control systems and approaches, the reader is referred to [29] and the references therein.

Most of the above works deal with overactuated vehicles, which have redundancy on the actuators and can reconfigure the forces and moments to keep the vehicle overactuated, or which become underactuated but with enough control actions to keep an adequate behaviour and compensate for the failure. In contrast to the previous references, the work at hand studies the case in which the vehicle is underactuated even in its nominal operation, similarly to previous works of the authors involving marine vehicles, both for control and identification [30]–[34]. In this kind of vehicles a failure or malfunction may cause a dramatic reduction of the control actions that can be applied over the vehicle. Thus, the scenario in which a critical failure reduces the available DOF of an underactuated vehicle is studied. Moreover, we consider the extreme situation in which only one thruster is available to control the vehicle dynamics. In this situation, a constant input on the available thruster will provoke the vehicle to turn in circles. Therefore, the design of an adequate control law so that the resulting trajectory, in average terms, follows a desired direction and drives the vehicle to a safe point is of the utmost importance. Considering that a discrete set of control inputs can be applied to the remaining thruster, namely two control inputs for the scenario at hand, the objective is to design the switching times of these control actions so that the vehicle moves in a spiral-like path, which follows, in average, a desired trajectory. This allows to define not only a simple, but also a robust and effective control law that drives the AUV towards a desired target point. The strategy proposed can be applied to multiple vehicles since it does not need a detailed model of the vehicle, and it does not require an accurate control parameters tuning, providing satisfactory results even for non optimal parameters.

Therefore, the contributions of the present work are threefold:

- i) A control strategy is proposed to drive underactuated vehicles to a safe recovery point in the extreme situation in which only one thruster is in operational conditions. The control strategy allows to drive the vehicle towards a desired direction, following a spiral-like path that will depend on the set of forces applied to the available thruster.
- ii) The limit case in which the only remaining thruster is controlled with just two control actions is considered. This assumption looks for a simple and effective control law that can be applied to multiple vehicles and situations, and also to consider the alternative scenario in which the remaining thruster has also a malfunction and only a discrete set of control actions can be applied.



FIGURE 1. MEDUSA class AUV.

- iii) The stability of the control law proposed, and the convergence of the trajectory to a neighbourhood of the desired target point are demonstrated analytically.

The paper is organized as follows. In Section II the notation, problem formulation, and the kinematics and dynamics models are presented. In Section III the control law to drive the vehicle to a safe recovery point in case of critical failure is proposed. In addition, the ability and stability of the control law to drive the vehicle along a desired average direction and to keep the vehicle in the vicinity of a selected recovery point are analyzed and demonstrated analytically. The main results are illustrated in Section IV where the good performance of the control law is shown through several simulations under different conditions. Finally, in Section V the conclusions and future work are presented.

II. PROBLEM FORMULATION

A. NOTATION

For the sake of completeness and to ease the readability of the forthcoming sections, in Table 1 the different symbols and variables used for the theoretical analysis are described. Notice, that these symbols and variables are also defined along the paper at their first appearance.

B. VEHICLE'S MODEL

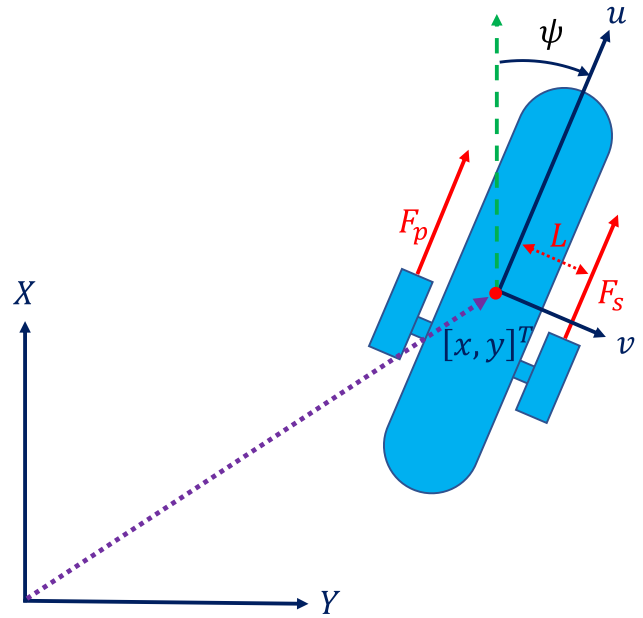
Consider an AUV composed of two missile shape bodies such as the MEDUSA Class AUV depicted in Figure 1. This kind of vehicle, which has two frontal thrusters to control surge speed and yaw rate, and two vertical thrusters for depth control, is underactuated. The AUV has positive buoyancy, which implies that in case of failure, it will emerge without the need of additional control actions. For this reason, the emergency control of the vehicle is studied in the horizontal plane, i.e. in 2D, once the vehicle is at the sea surface.

Following the standard convention [35], the origin of the AUV body-frame is located at its centre of mass, Figure 2. The speeds of the vehicle referred to the body-frame are

TABLE 1. Symbols and meaning.

Symbol	Meaning
$\mathbf{X} = [x, y]^T, \mathbf{X}_r$	XY-plane position and reference position
x_t, y_t	Transitory positions
$\psi, \dot{\psi}_t, \psi^*$	Orientation, transitory orientation and fixed point orientation of the vehicle
ψ_f	Limit of the transitory orientation: $\lim_{t \rightarrow \infty} \psi_t$
e_ψ	Transitory orientation error: $\psi_t - \psi_f$
$x' y' \psi'$	Positions and orientation under a reference frame rotation of angle ρ
$\boldsymbol{\nu} = [u, v, r]^T$	Body-frame vehicle's speeds: surge, sway and yaw rate
r_{min}, r_{max}	Minimum and maximum yaw rate
$\boldsymbol{\nu}_t, \boldsymbol{\nu}_e, \boldsymbol{\nu}_e^\pm$	Body-frame transitory vehicle's speeds, equilibrium vehicle's speeds for $a_p = a_0$ and for $a_p = a_0 \pm \Delta a$, respectively
$\boldsymbol{\nu}^* = [u^*, v^*, r^*]$	Fixed point speeds under control law (11)
$\mathbf{V} = [\dot{x}, \dot{y}]^T, \bar{\mathbf{V}}$	XY plane velocity vector and average velocity
V, V_{max}, V_c	Speed, maximum speed and current speed
V_{xf}, V_{yf}, V_f	Average final speeds: X-axis speed, Y-axis speed, and total speed, respectively.
V_e, R_e	Stationary equilibrium speed and turning radii when a constant control action a_0 is applied
a_s, a_p	Starboard and port thrusters control actions
a_0, a_m	Constant and maximum controller action
F_s, F_p	Starboard and port forces
τ, F	Torque and total force
L	Distance of the thrusters to the symmetry axis
m_u, m_v, m_{uv}, m_r	Mass and inertia constants
$\mathcal{D}_u, \mathcal{D}_v, \mathcal{D}_r$	Drag coefficients
\mathcal{K}	Proportional constant of the thrusters
$\mathcal{X}_u, \mathcal{X}_{ u }, \mathcal{Y}_v, \mathcal{Y}_{ v }, \mathcal{N}_r, \mathcal{N}_{ r }$	Hydrodynamic coefficients
Δa	Constant perturbation applied to the control action
$\Delta\psi, \hat{\Delta}\psi$	Orientation offset, and its empirical estimation
ψ_r	Desired average reference direction of movement
t, t_s, T	Time, transient time and time period
t_n	Times at which the control action switches
t_n^*	Times at which the control action switches in the fixed point trajectory
t_{end}	Time at which the control law stops switching
Δt_n	Interval of time between consecutive switches
Δt_n	$t_{n+1} - t_n$
$\Delta t_1, \Delta t_2$	Limits as $n \rightarrow \infty$ of Δt_{2n} and Δt_{2n+1} respectively
$[\Delta x_n, \Delta y_n]^T$	Distance covered between two consecutive control switches
δ_n, δ_m	Difference between ψ_r in two consecutive switches and bound of $ \delta_n $, respectively
d_n	Distance from the vehicle's position to the target point at t_n
d_{lim}	Limit distance to the target such that if $d_n \leq d_{lim}$ then $d_{n+1} < d_n$
D_n, D_{max}	Distance between two consecutive switching positions and maximum "diameter" of the trajectory
$\boldsymbol{\nu}_n, \boldsymbol{\nu}'_n$	Velocities at switching time t_n starting from two different initial conditions
∇	Lyapunov function
$c_i, \alpha_1, \alpha_2, \alpha, \varepsilon_i$	Positive constants
β	Function of class KL
$\mathbf{f}(\mathbf{x}), \mathbf{g}(\mathbf{x})$	Vector functions of the state
$\gamma(t), \delta(t), g(t)$	Scalar functions of time
$\gamma(t)$	Vector function of time
$\xi_1, \xi_2, \xi_x, \xi_y$	Transitory functions of time
g_m	Bound of function $g(t_n)$

$\boldsymbol{\nu} = [u, v, r]^T$, where u is surge speed, v is sway speed, and r is yaw rate. The velocity in the inertial frame is $\mathbf{V} = [\dot{x}, \dot{y}]^T$, where \dot{x} is the speed along the X-axis and \dot{y} is the speed along

**FIGURE 2.** Graphical representation of the forces applied to the AUV by the thrusters, AUV speeds in the body-frame and AUV position in the inertial coordinate frame.

the Y-axis. Finally ψ is the angle that the vehicle orientation forms with the X-axis and its derivative $\dot{\psi} = r$ is the yaw rate. Then, in the absence of ocean currents, the kinematic model of the vehicle yields

$$\dot{x} = u \cdot \cos(\psi) - v \cdot \sin(\psi) \quad (1)$$

$$\dot{y} = u \cdot \sin(\psi) + v \cdot \cos(\psi) \quad (2)$$

$$\dot{\psi} = r \quad (3)$$

As mentioned above, in the 2D scenario considered and under normal operation, the vehicle is controlled by two frontal thrusters whose inputs are a_s and a_p , which are normalized reference commands for the internal controller of the propellers in the range [-100 100], i.e., the angular speed reference for the starboard and port thrusters, respectively. Then, each propeller produces a force that is proportional to the square of its own angular speed, which is positive (push forward) when the control action is positive, and negative (push backward) when the control action is negative. Thus, the forces F_s and F_p produced by each thruster in response to the control actions are:

$$F_s(a_s) = \mathcal{K} \cdot |a_s| \cdot a_s$$

$$F_p(a_p) = \mathcal{K} \cdot |a_p| \cdot a_p$$

where \mathcal{K} is the proportional constant which relates control actions to thrust. Then the total force is the summation of the force provided by each of the thrusters, $F = F_p(a_p) + F_s(a_s)$, which also produces the torque $\tau = L \cdot (F_p(a_p) - F_s(a_s))$, being L the distance of each of the thrusters to the symmetry axis of the vehicle.

In the emergency situation studied it is assumed that one of the thrusters becomes faulty and cannot be operated.

For the sake of simplicity, and without loss of generality, the starboard thruster has been considered as the faulty one, and $a_s = 0$, $F_s(a_s) = 0$. Thus, only the control action a_p is available, and the total force and torque become $F = F_p(a_p)$ and $\tau = LF_p(a_p)$, respectively, allowing only a partial control of the surge speed and the yaw angle. Therefore, according to [36], [37] and given the above constraint, the dynamics of the vehicle yields

$$m_u \cdot \dot{u} - m_v \cdot v \cdot r + \mathcal{D}_u \cdot u = F = F_p(a_p) \quad (4)$$

$$m_v \cdot \dot{v} + m_u \cdot u \cdot r + \mathcal{D}_v \cdot v = 0 \quad (5)$$

$$m_r \cdot \dot{r} - m_{uv} \cdot u \cdot v + \mathcal{D}_r \cdot r = \tau = L \cdot F_p(a_p) \quad (6)$$

where m_u , m_v and m_r are the mass and inertia constants (mass of the vehicle plus added masses that arise from the interaction with the surrounding water), and $m_{uv} = m_u - m_v$. The Coriolis terms $v \cdot r$, $u \cdot r$, and $u \cdot v$ are caused by the fact that the body frame is rotating.

Finally, the terms $\mathcal{D}_u = -\mathcal{X}_u - \mathcal{X}_{|u|} \cdot |u|$, $\mathcal{D}_v = -\mathcal{Y}_v - \mathcal{Y}_{|v|} \cdot |v|$, and $\mathcal{D}_r = -\mathcal{N}_r - \mathcal{N}_{|r|} \cdot |r|$ are caused by the dissipating forces of the water, where \mathcal{X}_u , $\mathcal{X}_{|u|}$, \mathcal{Y}_v , $\mathcal{Y}_{|v|}$, \mathcal{N}_r , $\mathcal{N}_{|r|}$, are the hydrodynamic coefficients, which are negative and then \mathcal{D}_u , \mathcal{D}_v and \mathcal{D}_r are positive.

Therefore, the objective is to design a control action over a_p so that the system (1)-(6) converges to a neighbourhood of the origin from any initial condition, i.e., the AUV can be driven with the use of a single thruster to a desired (recovery) area.

III. CONTROL DESIGN

The AUV velocity and position control are derived for the case in which a critical thruster failure occurs and only one thruster is available. Moreover, this remaining available thruster may also have a limited set of actions due to possible additional damage.

Notice that all the state variables $x(t)$, $y(t)$, $\psi(t)$, $u(t)$, $v(t)$ and $r(t)$ are time-dependent functions. Nevertheless, in the following, for the sake of clarity and with an abuse of notation, the explicit indication that the state variables are time-dependent will be omitted when there is no ambiguity.

A. AVERAGE VELOCITY CONTROL

In the situation where one of the horizontal thrusters is not working, the AUV should be controlled and driven to a desired safety point. Then, a control action such that the vehicle moves, *in average*, towards a desired direction must be defined. It is important to notice that, as the single control action a_p is used and it impacts directly on both the surge speed u and the yaw rate r , it is not possible to make the vehicle follow a straight path with a certain desired reference surge speed and orientation, as it would be expected if both control actions a_s and a_p could be applied.

This fact can be seen by noticing that a constant orientation ψ implies that $r = 0$, by Eq. (3). Thus, (5) becomes $m_v \dot{v} + \mathcal{D}_v v = 0$, which has a global asymptotically stable equilibrium point at $v = 0$. The latter is straightforward to

prove by considering the Lyapunov function $\mathbb{V} = v^2/2$, where $\dot{\mathbb{V}} = -\frac{\mathcal{D}_v}{m_v} \cdot v^2 < 0$.

However, Eq. (6) becomes $-m_{uv} \cdot u \cdot v = \tau = L \cdot F_p(a_p)$, where the left hand side tends to 0 as $t \rightarrow \infty$, so $F_p(a_p) \rightarrow 0$. Therefore, $u \rightarrow 0$ too, since (4) reduces to $m_u \cdot \dot{u} + \mathcal{D}_u \cdot u = 0$ which is also globally asymptotically stable, and it is not possible to converge to a sustainable forward velocity with constant orientation.

At this point, it is important to analyze the AUV behaviour when a constant control action $a_p = a_0$ is applied. In this situation, the equilibrium solution of (4)-(6) is $\mathbf{v}_e = [u_e, v_e, r_e]^T$:

$$-m_v \cdot v_e \cdot r_e + \mathcal{D}_u(u_e) \cdot u_e = F_p(a_0) \quad (7)$$

$$m_u \cdot u_e \cdot r_e + \mathcal{D}_v(v_e) \cdot v_e = 0 \quad (8)$$

$$-m_{uv} \cdot u_e \cdot v_e + \mathcal{D}_r(r_e) \cdot r_e = L \cdot F_p(a_0) \quad (9)$$

Let's suppose that this equilibrium point is globally asymptotically and exponentially stable. In a normal situation, this is usually true since vehicles are designed to have a stable dynamics for constant control actions (the existence of such points will be shown later in Lemma 4).

The yaw rate equation in the time domain can be written as $r(t) = r_e + r_t$, where r_t is a transitory term that, due to the exponential convergence, can be bounded as $|r_t| = |r(t) - r_e| \leq \|\mathbf{v}(t) - \mathbf{v}_e\| \leq c_1 \|\mathbf{v}(0) - \mathbf{v}_e\| e^{-c_2 t}$, being c_1 and c_2 two positive constants. Thus, the yaw angle can be defined as $\psi(t) = \int_0^t (r_e + r_t) dt = r_e t + \int_0^t r_t dt = r_e t + \psi_t$, where ψ_t is a transitory term that converges to a fixed value ψ_f as $t \rightarrow \infty$, $\psi_{t \rightarrow \infty} = \int_0^\infty r_t dt = \psi_f$. This transitory yaw angle ψ_t can be bounded as $|\psi_t| \leq \int_0^\infty |r_t| \leq \int_0^\infty c_1 \|\mathbf{v}(0) - \mathbf{v}_e\| e^{-c_2 t} = \frac{c_1}{c_2} \|\mathbf{v}(0) - \mathbf{v}_e\|$. Thus, the average angular speed yields

$$\bar{r} = \lim_{t \rightarrow \infty} \frac{1}{t} \int_0^t (r_e + r_t) ds = r_e + \lim_{t \rightarrow \infty} \frac{\psi_t}{t} = r_e.$$

The same analysis holds for $u(t)$ and $v(t)$, considering u_t and v_t the transitory terms of the surge speed and sway speed, respectively.

Therefore, from Eq. (1), the average velocity over the X-axis of the inertial reference frame can be computed as:

$$\bar{x} = \lim_{t \rightarrow \infty} \frac{1}{t} \int_0^t ((u_e + u_t) \cdot \cos(r_e \cdot s + \psi_t) - (v_e + v_t) \cdot \sin(r_e \cdot s + \psi_t)) ds \quad (10)$$

By letting $e_\psi = \psi_t - \psi_f$, the first term of the integral in (10) can be rewritten as:

$$\begin{aligned} & \cos(r_e \cdot s + \psi_t) \\ &= \cos(r_e \cdot s + \psi_f + e_\psi) \\ &= \cos(r_e \cdot s + \psi_f) \cos(e_\psi) - \sin(r_e \cdot s + \psi_f) \sin(e_\psi) \\ &= \cos(r_e \cdot s + \psi_f) + \cos(r_e \cdot s + \psi_f)(\cos(e_\psi) - 1) \\ &\quad - \sin(r_e \cdot s + \psi_f) \sin(e_\psi) = \cos(r_e \cdot s + \psi_f) + \xi_1(s) \end{aligned}$$

where $\xi_1(s)$ tends exponentially to zero as $s \rightarrow \infty$ since ψ_t tends exponentially to ψ_f , so $e_\psi \rightarrow 0$. Following similar computations, the second term in (10) yields $\sin(r_e \cdot s + \psi_t) = \sin(r_e \cdot s + \psi_f) + \xi_2(s)$, where $\xi_2(s)$ also tends exponentially

to zero as $s \rightarrow \infty$, and thus, the average velocity over the X-axis of the inertial reference frame becomes:

$$\begin{aligned}\bar{x} &= \lim_{t \rightarrow \infty} \frac{1}{t} \int_0^t ((u_e + u_t) \cos(r_e \cdot s + \psi_t) \\ &\quad - (v_e + v_t) \sin(r_e \cdot s + \psi_t)) ds \\ &= \lim_{t \rightarrow \infty} \frac{1}{t} \int_0^t (u_e \cos(r_e s + \psi_f) - v_e \sin(r_e s + \psi_f)) ds \\ &\quad + \lim_{t \rightarrow \infty} \frac{1}{t} \int_0^t (u_t \cos(r_e s + \psi_f) - v_t \sin(r_e s + \psi_f)) ds \\ &\quad + \lim_{t \rightarrow \infty} \frac{1}{t} \int_0^t (u_e + u_t) \xi_1(s) + (v_e + v_t) \xi_2(s) ds \\ &= \lim_{t \rightarrow \infty} \frac{1}{t} \int_0^t (u_e \cos(r_e s + \psi_f) - v_e \sin(r_e s + \psi_f)) ds \\ &= 0\end{aligned}$$

Notice that this average speed is zero because the integral of exponentially decreasing functions are bounded, and the trigonometric functions that are periodic with zero average over a period are also bounded. The same analysis holds for \bar{y} , the average speed over the Y-axis of the inertial reference frame. This result has an intuitive explanation. Notice that when enough time has passed, the vehicle will move with constant speed $V_e = \sqrt{u_e^2 + v_e^2}$ and constant angular velocity r_e . Thus, the trajectory will be a circle of radii $R_e = \frac{V_e}{r_e}$, and the average advance velocity is zero.

In order to obtain an non-zero average advance velocity, the symmetry of the circular trajectory must be broken, so a constant input control action is not suitable. The following control law is proposed:

$$a_p = a_0 + \Delta a \cdot \text{sign}(\sin(\psi)) \quad (11)$$

The concept within (11) is that the control action will be different when the vehicle is oriented to East ($\sin(\psi) > 0$) than when the vehicle is oriented to West ($\sin(\psi) < 0$) breaking the symmetry of the circular trajectory, see Fig. 3. Notice that the sign of the control law (11) changes when $\psi = n\pi$, with $n = 0, 1, 2, \dots$. The value of ψ for changing the sign of (11) has been chosen for simplicity of explanation, and any other angle could be chosen without loss of generality. In fact, the selected angle will depend on the desired direction of movement, as it will be shown in the forthcoming analysis.

The control law works as follows: Consider that the vehicle turns clockwise ($r > 0$) describing an approximately circular trajectory (for Δa small) and pointing to the interior of the circular path because $u > 0$ and $v < 0$. Therefore, the velocity vector of the vehicle, which is tangent to the trajectory, points to port. When $\psi = 2n\pi$ the vehicle points exactly to the North, which is the frontier at which the vehicle changes its orientation from West to East (point A of Figure 3), and a_p switches from $a_p = a_0 - \Delta a$ to $a_p = a_0 + \Delta a$, following the red path of Figure 3. Once ψ reaches $(2n+1)\pi$, the vehicle points exactly to the South (point B of Figure 3) and the control law switches again to $a_p = a_0 - \Delta a$, describing the blue path. Since the control action is different in both parts of the path (red and blue) the trajectory does not close,

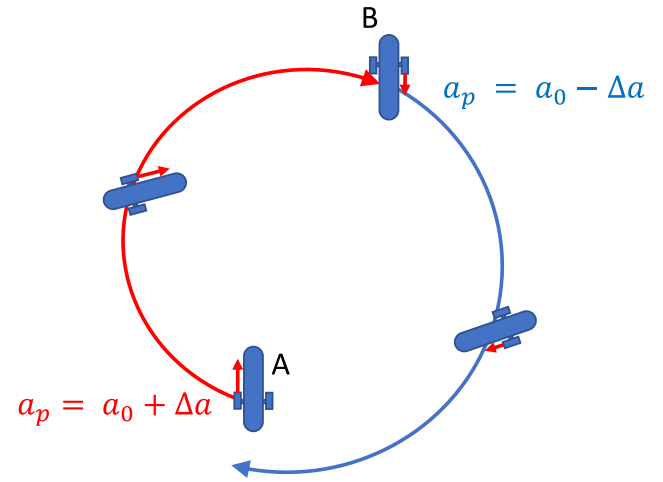


FIGURE 3. Behaviour of control law (11).

i.e. it is not a circumference. Thus, the vehicle moves in “some” direction, which depends on the angle or condition to switch the control law. This pattern is repeated periodically producing an average movement of the vehicle on a certain course.

In order to prove the above statement, and before starting the stability analysis of the control law proposed, we must resort to some technical results:

Lemma 1: Consider system $\dot{\mathbf{x}} = \mathbf{f}(\mathbf{x})$ such that \mathbf{x}_e is an exponentially stable equilibrium point of the system and the first derivative of \mathbf{f} is bounded and Lipschitz on \mathbf{x} in a domain $\|\mathbf{x} - \mathbf{x}_e\| < c_0$, where c_0 is a positive constant. Let $\mathbf{x}_1(t)$ and $\mathbf{x}_2(t)$ be two solutions of the differential equation with initial conditions $\mathbf{x}_1(t_0)$ and $\mathbf{x}_2(t_0)$, respectively. Then $\|\mathbf{x}_2(t) - \mathbf{x}_1(t)\| < c_1 e^{-c_2(t-t_0)} \|\mathbf{x}_2(t_0) - \mathbf{x}_1(t_0)\|$ for $t > t_0$, being c_1 and c_2 two positive constants.

Proof: This is a simple application of Theorem 9.1 from [38] for the unperturbed case $\mathbf{g}(\mathbf{x}) = 0$ in equation 9.6 of [38]), when, in addition, the system is autonomous. \square

Lemma 2: Consider system $\dot{\mathbf{x}} = \mathbf{f}(\mathbf{x}, a_p)$ continuously differentiable and locally Lipschitz in a domain $\|\mathbf{x}\| < c_3 + \varepsilon_1$, where c_3 is a positive constant and ε_1 is a small positive constant. Suppose also that the solutions of the system are globally uniformly ultimately bounded (GUUB) with bound c_3 for $0 \leq a_p \leq a_m$. Then, $\|\mathbf{x}(t)\| \leq \beta(\|\mathbf{x}(t_0)\|, t - t_0) + c_4 a_m$ for some positive constant c_4 and a function β of class KL, i.e. β is a non decreasing function of its first argument, and decreasing on the second argument, such that $\beta \rightarrow 0$ as $t \rightarrow \infty$.

Proof: The solutions of the system are GUUB with bound c_3 so, for each initial condition there exists a function β_1 of class KL such that $\|\mathbf{x}(t)\| \leq \beta_1(\|\mathbf{x}(t_0)\|, t - t_0) + c_3$ for $t > t_0$. Since $\beta_1 \rightarrow 0$ as $t \rightarrow \infty$, there exists a time $t_s = t_s(\|\mathbf{x}(t_0)\|)$ such that $\beta_1(\|\mathbf{x}(t_0)\|, t_s - t_0) < \varepsilon_1$. Then for $t \geq t_s$, $\|\mathbf{x}(t)\| \leq c_3 + \varepsilon_1$.

Thus, before time t_s , as $a_p \leq a_m$, we know that \mathbf{x} lies in the region where \mathbf{f} is Lipschitz, and following the same arguments

of the proof of Lemma 4.6 of [38], we obtain that $\|\mathbf{x}(t)\| \leq \beta_2(\|\mathbf{x}(t_s)\|, t - t_s) + c_4 a_m$ for $t \geq t_s$ and β_2 of class *KL*. Therefore, all the vanishing terms can be bounded by a single *KL* function β and the condition of the theorem holds for all $t \geq t_0$. \square

Lemma 3: Consider system $\dot{\mathbf{v}} = \mathbf{f}(\mathbf{v}, a_p)$ defined by equations (1)-(6), where $\mathbf{v} = [u, v, r]$. Let $\mathbf{v}_e = [u_e, v_e, r_e]$ be the equilibrium solution of the system for $a_p = a_0 > 0$, then $u_e, r_e > 0$, $v_e < 0$ and the Jacobian $\frac{d\mathbf{f}}{d\mathbf{v}}$ is continuous and Lipschitz in a neighbourhood of \mathbf{v}_e .

Proof: Due to the presence of absolute values in the drag terms \mathcal{D}_u , \mathcal{D}_v and \mathcal{D}_r on model (4)-(6), the Jacobian matrix of the system is not differentiable when u , v or r are zero. In the rest of domain the system is smooth. Let's prove by contradiction that for $a_0 > 0$, the equilibrium solutions are such that $u_e \neq 0$, $v_e \neq 0$ and $r_e \neq 0$.

Suppose that $u_e = 0$, then (8) becomes $\mathcal{D}_v(v_e) \cdot v_e = 0$ and thus, $v_e = 0$. It implies that, given (7), $F_p(a_0) = 0$ and $a_0 = 0$, which is a contradiction, and demonstrates that $u_e \neq 0$.

Now suppose that $v_e = 0$. Then, (8) becomes $m_u \cdot u_e \cdot r_e = 0$, which implies that $r_e = 0$ because it is already known that $u_e \neq 0$. However, given (9), $L \cdot F_p(a_0) = 0$, which is also a contradiction, and then $v_e \neq 0$.

Finally, suppose that $r_e = 0$. Given (8), it yields $v_e = 0$, which is again a contradiction and $r_e \neq 0$.

To check that the signs of the speeds are correct, consider the linearization of (7) and (9) around the equilibrium point \mathbf{v}_e :

$$|\mathcal{X}_u| \cdot u_e = F_p(a_0) \quad (12)$$

$$|\mathcal{N}_r| \cdot r_e = L \cdot F_p(a_0) \quad (13)$$

Since $F_p > 0$, then u_e and r_e exist and are positive for small enough a_0 , as shown by the inverse function theorem (see [39], theorem 7-5). Equation (8) yields $\mathcal{D}_v(v_e) \cdot v_e = -m_u \cdot u_e \cdot r_e < 0 \rightarrow v_e < 0$, so the signs are correct. In addition, as the speeds are only zero for $a_0 = 0$, they must remain with the same sign for $a_0 > 0$. \square

Lemma 4: Consider the system $\dot{\mathbf{v}} = \mathbf{f}(\mathbf{v}, a_p)$ defined by equations (1)-(6). There exists an a_m such that if $0 \leq a_p \leq a_m$, then the equilibrium point \mathbf{v}_e for $a_p = a_0$ is globally exponentially stable, i.e., there exist positive constants c_1 and c_2 such that $\|\mathbf{v}(t) - \mathbf{v}_e\| < c_1 e^{-c_2(t-t_0)} \|\mathbf{v}(t_0) - \mathbf{v}_e\|$ for $t > t_0$. Moreover $c_1 e^{\frac{-\pi c_2}{r_e}} < 1$.

Proof: Consider the Lyapunov function $\mathbb{V} = \frac{1}{2}(m_u u^2 + m_v v^2 + m_r r^2)$ which represents the kinetic energy of the vehicle and the surrounding water. Then, $c_5 \|\mathbf{v}\|^2 \leq \mathbb{V} \leq c_6 \|\mathbf{v}\|^2$ where $c_5 = \frac{1}{2} \min(m_u, m_v, m_r)$ and $c_6 = \frac{1}{2} \max(m_u, m_v, m_r)$. The derivative of \mathbb{V} becomes:

$$\begin{aligned} \dot{\mathbb{V}} &= -\mathcal{D}_u u^2 - \mathcal{D}_v v^2 - \mathcal{D}_r r^2 + u F_p(a_p) + r L F_p(a_p) \\ &\leq -|\mathcal{X}_u| u^2 - |\mathcal{Y}_v| v^2 - |\mathcal{N}_r| r^2 + \|\mathbf{v}\|(1+L)F_p(a_p) \\ &\leq -\min(|\mathcal{X}_u|, |\mathcal{Y}_v|, |\mathcal{N}_r|) \|\mathbf{v}\|^2 + \|\mathbf{v}\|(1+L)F_p(a_p) \\ &\leq -c_7 \|\mathbf{v}\|^2 + \|\mathbf{v}\|(1+L)F_p(a_p) \end{aligned} \quad (14)$$

From theorem 4.10 of [38], the system (4)-(6) is globally exponentially stable when $a_p = 0$. Furthermore, if a_p is bounded, i.e., $0 \leq a_p \leq a_m$, then (14) is negative if $\|\mathbf{v}\| \geq \frac{(1+L)F_p(a_m)}{c_7}$ and $c_7 = \min(|\mathcal{X}_u|, |\mathcal{Y}_v|, |\mathcal{N}_r|)$. Therefore, the system is Input to State Stable (ISS) with respect to a_p by theorem 4.19 of [38]. In addition, since $\|\frac{\partial \mathbb{V}}{\partial \mathbf{v}}\| \leq 2c_6 \|\mathbf{v}\|$, and considering the special case of $\gamma(t) = 0$ and $\delta(t) = (1+L)F_p(a_m)$ in Lemma 9.4 of [38], we obtain:

$$\begin{aligned} \|\mathbf{v}(t)\| &\leq \sqrt{\frac{c_6}{c_5}} \|\mathbf{v}(t_0)\| e^{-\frac{c_7}{2c_6}(t-t_0)} \\ &\quad + \frac{c_6(1+L)}{2c_5} F_p(a_m) \int_{t_0}^t e^{-\frac{c_7}{2c_6}(t-s)} ds \\ &\leq \sqrt{\frac{c_6}{c_5}} \|\mathbf{v}(t_0)\| e^{-\frac{c_7}{2c_6}(t-t_0)} \\ &\quad + \frac{c_6^2(1+L)}{c_5 c_7} F_p(a_m) \left[1 - e^{-\frac{c_7}{2c_6}(t-t_0)} \right] \\ &\leq c_1 \|\mathbf{v}(t_0)\| e^{-c_2(t-t_0)} + \frac{c_6^2(1+L)}{c_5 c_7} F_p(a_m) \end{aligned}$$

This proves that the convergence to a neighbourhood of the origin is exponential, so letting $a_p = a_0$ small enough, the linearization of the system could be as close as desired to the linearization around the origin (since the Jacobian matrix is continuous). Then, the trajectory converges exponentially to the attractive region of the linear system, and the equilibrium point is globally exponentially stable.

Finally, $r_e(a_0) \rightarrow 0$ as $a_0 \rightarrow 0$, so $c_1 e^{\frac{-\pi c_2}{r_e(a_0)}} \rightarrow c_1 e^{-\infty} = 0$. Thus, a_0 can be chosen so that $c_1 e^{\frac{-\pi c_2}{r_e}} < 1$. \square

Now we have the necessary tools to analyse the behaviour of the control law (11).

Lemma 5: Consider system (1)-(6) under control action (11), then it is possible to choose a_0 and Δa such that the velocities of the system converge to an exponentially stable limit cycle of sustained oscillation and, in addition the average velocity of the system also converges exponentially to a stable fixed value $[\bar{x}, \bar{y}]^T \rightarrow [V_{xf}, V_{yf}]^T \neq 0$.

Proof: As shown by Lemma 4, given a control action $a_p = a_0$ and a bounded disturbance Δa small enough so that $0 < a_0 - \Delta a < a_0 < a_0 + \Delta a < a_m$, then, the system (4)-(6) has globally exponentially stable equilibrium points at $\mathbf{v}_e = [u_e, v_e, r_e]$, $\mathbf{v}_e^+ = [u_e^+, v_e^+, r_e^+]$ and $\mathbf{v}_e^- = [u_e^-, v_e^-, r_e^-]$ for $a_p = a_0$, $a_p = a_0 + \Delta a$ and $a_p = a_0 - \Delta a$, respectively. In addition, all the three equilibrium points satisfy $c_1 e^{\frac{-\pi c_2}{r_e}} < 1$.

Lemma 3 shows that the solutions are GUUB and the system is locally Lipschitz in any bounded region, thus, Lemma 2 implies that $\mathbf{v}(t)$ will converge to a neighbourhood of \mathbf{v}_e than can be made arbitrary small. Therefore, without loose of generality, we can start the analysis at time t_0 such that $\|\mathbf{v} - \mathbf{v}_e\| \leq c_4 \Delta a$, where c_4 is the positive constant of Lemma 2.

The yaw rate equation can be expressed as $r(t) = r_e^\pm + r_t$, where r_t is a transitory function that tends to zero when a_p is constant. Using the exponential convergence, and the fact

that $\|\mathbf{v} - \mathbf{v}_e\| \leq c_4 \Delta a$, it yields $|r_t| \leq c_1 c_4 \Delta a$, and therefore, $0 \leq r_{min} \leq r(t) \leq r_{max}$ where $r_{min} = \min(r_e^+, r_e^-) - c_1 c_4 \Delta a$ and $r_{max} = \max(r_e^+, r_e^-) + c_1 c_4 \Delta a$, being both positive if Δa is small enough.

Since $r(t)$ is bounded and positive, then $\psi(t)$ is strictly increasing and there exists a sequence of times t_n such that $\psi(t_n) = n\pi$, for $n = 1, 2, \dots$. These are precisely the times at which the control action a_p switches from $a_0 - \Delta a$ to $a_0 + \Delta a$ when n is even, or from $a_0 + \Delta a$ to $a_0 - \Delta a$ when n is odd.

Now, consider the trajectory that starts at $\mathbf{v}_n = \mathbf{v}(t_n)$, being t_n an even switching time. During some time the control action $a_p = a_0 + \Delta a$ will remain constant, and the angle ψ will increase from $\psi(t_n) = n\pi$ to $\psi(t_{n+1}) = (n+1)\pi$, so:

$$\begin{aligned}\pi &= \psi(t_{n+1}) - \psi(t_n) = \int_{t_n}^{t_{n+1}} r(s) ds \\ &= r_e^+ \Delta t_n + \int_{t_n}^{t_{n+1}} r_t ds\end{aligned}\quad (15)$$

where Δt_n is the time interval between two consecutive switches of the control action, i.e., $\Delta t_n = t_{n+1} - t_n$, and $r_t = r - r_e^+$, which implies

$$\frac{\pi - \int_{t_n}^{t_{n+1}} |r_t| ds}{r_e^+} \leq \Delta t_n \leq \frac{\pi + \int_{t_n}^{t_{n+1}} |r_t| ds}{r_e^+}$$

Taking into account the exponential convergence $\int_{t_n}^{t_{n+1}} |r_t| ds \leq \int_0^\infty c_1 c_4 \Delta a e^{-c_2 s} ds \leq \frac{c_1 c_4 \Delta a}{c_2}$, we obtain:

$$\frac{\pi - \frac{c_1 c_4 \Delta a}{c_2}}{r_e^+} \leq \Delta t_n \leq \frac{\pi + \frac{c_1 c_4 \Delta a}{c_2}}{r_e^+}$$

At switching time t_{n+1} the system reaches the state \mathbf{v}_{n+1} . Consider now another trajectory that starts at \mathbf{v}'_n at the same starting time t_n and ends on state $\mathbf{v}'_{n+1} = \mathbf{v}'(t'_{n+1})$ at a slightly different switching time t'_{n+1} , then:

$$\begin{aligned}\mathbf{v}'_{n+1} - \mathbf{v}_{n+1} &= \mathbf{v}'(t'_{n+1}) - \mathbf{v}(t_{n+1}) \\ &= \mathbf{v}'(t_{n+1}) - \mathbf{v}(t_{n+1}) + \mathbf{v}'(t'_{n+1}) - \mathbf{v}'(t_{n+1})\end{aligned}\quad (16)$$

As (15) also holds for t'_{n+1} , then by subtracting both Eqs. (15) for t'_{n+1} and t_{n+1} , and assuming without loss of generality that $t'_{n+1} \geq t_{n+1}$ (on the contrary, just interchange the roles between \mathbf{v} and \mathbf{v}'), we obtain:

$$\begin{aligned}0 &= \pi - \pi = \int_{t_n}^{t'_{n+1}} r'(s) ds - \int_{t_n}^{t_{n+1}} r(s) ds \\ &= \int_{t_{n+1}}^{t'_{n+1}} r'(s) ds - \int_{t_n}^{t_{n+1}} (r'(s) - r(s)) ds\end{aligned}$$

and therefore:

$$\begin{aligned}(t'_{n+1} - t_{n+1}) r_{min} &\leq \int_{t_{n+1}}^{t'_{n+1}} r'(s) ds \\ &= \int_{t_n}^{t_{n+1}} (r'(s) - r(s)) ds\end{aligned}$$

Then, by Lemma 3, the conditions of Lemma 1 hold:

$$\begin{aligned}|t'_{n+1} - t_{n+1}| r_{min} &\leq \int_{t_n}^{t_{n+1}} |r'(s) - r(s)| ds \\ &\leq \int_{t_n}^{t_{n+1}} c_1 e^{-c_2(s-t_n)} \|\mathbf{v}'_n - \mathbf{v}_n\| ds \\ &\leq \int_{t_n}^\infty c_1 e^{-c_2(s-t_n)} \|\mathbf{v}'_n - \mathbf{v}_n\| ds \\ &\leq \frac{c_1}{c_2} \|\mathbf{v}'_n - \mathbf{v}_n\|\end{aligned}\quad (17)$$

Finally, by the mean value theorem (see [40] Ch.11 Theorem 4), $\frac{\mathbf{v}'(t'_{n+1}) - \mathbf{v}'(t_{n+1})}{t'_{n+1} - t_{n+1}} = \mathbf{f}(\mathbf{v}(t), a_0 + \Delta a)$ for some t between t'_{n+1} and t_{n+1} . Furthermore, as \mathbf{f} is locally Lipschitz with constant c_8 , we get $\|\mathbf{f}(\mathbf{v}(t), a_0 + \Delta a) - \mathbf{f}(\mathbf{v}_e^+(t_n), a_0 + \Delta a)\| = \|\mathbf{f}(\mathbf{v}(t), a_0 + \Delta a) - 0\| \leq c_8 \|\mathbf{v} - \mathbf{v}_e^+\| \leq c_8 c_4 \Delta a$. Thus $\|\mathbf{v}'(t'_{n+1}) - \mathbf{v}'(t_{n+1})\| \leq |t'_{n+1} - t_{n+1}| c_8 c_4 \Delta a$, and, considering again Lemma 1 with (16) and (17):

$$\begin{aligned}\|\mathbf{v}'_{n+1} - \mathbf{v}_{n+1}\| &\leq \|\mathbf{v}'(t_{n+1}) - \mathbf{v}(t_{n+1})\| \\ &\quad + \|\mathbf{v}'(t'_{n+1}) - \mathbf{v}'(t_{n+1})\| \\ &\leq c_1 e^{-c_2 \Delta t_n} \|\mathbf{v}'_n - \mathbf{v}_n\| + c_4 c_8 \Delta a |t'_{n+1} - t_{n+1}| \\ &\leq \left(c_1 e^{-c_2 \Delta t_n} + \frac{c_1 c_4 c_8 \Delta a}{c_2 r_{min}} \right) \|\mathbf{v}'_n - \mathbf{v}_n\| \\ &= \alpha_1 \|\mathbf{v}'_n - \mathbf{v}_n\|\end{aligned}\quad (18)$$

A similar analysis can be carried out for the transition from t_{n+1} to t_{n+2} , so finally:

$$\begin{aligned}\|\mathbf{v}'_{n+2} - \mathbf{v}_{n+2}\| &\leq \alpha_2 \|\mathbf{v}'_{n+1} - \mathbf{v}_{n+1}\| \\ &\leq \alpha_2 \alpha_1 \|\mathbf{v}'_n - \mathbf{v}_n\| = \alpha \|\mathbf{v}'_n - \mathbf{v}_n\|\end{aligned}\quad (19)$$

where $\alpha_2 = \left(c_1 e^{-c_2 \Delta t_{n+1}} + \frac{2 c_1 c_4 c_8 \Delta a}{c_2 r_{min}} \right)$. Note that the 2 factor in the term $\frac{2 c_1 c_4 c_8 \Delta a}{c_2 r_{min}}$ is consequence of the fact that in this case both $|t'_{n+1} - t_{n+1}|$ and $|t'_{n+2} - t_{n+2}|$ need to be bounded, as in (17). The constant α in (19) can be made less than one by selecting Δa small enough, i.e. if $\Delta a \rightarrow 0$, then $\alpha \rightarrow c_1^2 e^{-c_2 (\Delta t_{n+1} + \Delta t_n)} \rightarrow c_1^2 e^{-c_2 T} \leq c_1^2 e^{-\frac{2 c_2 \pi}{r_e}} = (c_1 e^{-\frac{c_2 \pi}{r_e}})^2 < 1$.

Equation (19) shows that the transition from two consecutive even switching times $t_{2n} \rightarrow t_{2n+2}$ is an exponential contraction mapping from the set $\|\mathbf{v} - \mathbf{v}_e\| < c_4 \Delta a$ to itself, and thus a fixed point \mathbf{v}^* exists such that if $\mathbf{v}_{2n} = \mathbf{v}^*(t_{2n})$ then $\mathbf{v}_{2n+2} = \mathbf{v}_{2n}$ by the Contraction Mapping theorem (Theorem B.1 of [38]).

This further implies that \mathbf{v}_{2n} tends exponentially fast to $\mathbf{v}^*(t_{2n})$ as $n \rightarrow \infty$ and, by the continuity of solutions over a bounded interval, Δt_{2n} and Δt_{2n+1} tend to constants Δ_1 and Δ_2 , respectively, and the solution $\mathbf{v}(t - t_{2n})$ for $t_{2n} \leq t \leq t_{2n} + \Delta_1 + \Delta_2$ tends to $\mathbf{v}^*(t) = [u^*(t), v^*(t), r^*(t)]^T$, which is the periodic solution of the system starting from $\mathbf{v}(0) = \mathbf{v}^*(0)$ with period $T = \Delta_1 + \Delta_2$. Thus the speeds tend exponentially to a stable limit cycle as stated by the theorem.

To conclude the proof, the average velocity can be computed following the same procedure of (10):

$$\begin{aligned}\bar{x} &= \frac{1}{T} \int_0^T (u^*(t) \cos(\psi^*(t)) - v^*(t) \sin(\psi^*(t))) dt \\ &= \frac{1}{T} \int_0^{2\pi} \left(\frac{u^*(\psi)}{r^*(\psi)} \cos(\psi) - \frac{v^*(\psi)}{r^*(\psi)} \sin(\psi) \right) d\psi = V_{xf}\end{aligned}\quad (20)$$

$$\begin{aligned}\bar{y} &= \frac{1}{T} \int_0^T (u^*(t) \sin(\psi^*(t)) + v^*(t) \cos(\psi^*(t))) dt \\ &= \frac{1}{T} \int_0^{2\pi} \left(\frac{u^*(\psi)}{r^*(\psi)} \sin(\psi) + \frac{v^*(\psi)}{r^*(\psi)} \cos(\psi) \right) d\psi = V_{yf}\end{aligned}\quad (21)$$

where the change of variables $\psi^*(t) = \psi, d\psi = r^*(\psi)dt$ has been applied. To verify that the average velocity can be chosen to be different from zero with a proper selection of a_0 consider the limit case in which a_0 is very small and $\Delta a \ll a_0$.

On the one hand, from (7) and (9) and expanding them up to the second order in a_0 and Δa , we obtain $u_e^\pm \approx \frac{1}{|\mathcal{X}_u|} F_p(a_0 \pm \Delta a)$ and $r_e^\pm \approx \frac{L}{|\mathcal{N}_r|} F_p(a_0 \pm \Delta a)$. Thus, $\frac{u_e^\pm}{r_e^\pm} = \frac{|\mathcal{X}_u|}{|\mathcal{N}_r| L}$, which implies that $\frac{u^*(\psi)}{r^*(\psi)}$ is constant (up to this order of approximation) and thus, the integral over a period of $\frac{u^*(\psi)}{r^*(\psi)} \cos(\psi)$ is zero.

On the other hand, from (8), $v_e^\pm \approx -\frac{m_u}{|\mathcal{Y}_v|} u_e^\pm r_e^\pm$, so $\frac{v_e^\pm}{r_e^\pm} = -\frac{m_u}{|\mathcal{Y}_v|} u_e^\pm = -\frac{m_u}{|\mathcal{Y}_v|} u_e \mp \frac{2Km_u}{|\mathcal{Y}_v \mathcal{X}_u|} a_0 \Delta a$. This implies that $\frac{v^*(\psi)}{r^*(\psi)}$ is a function that converges to two different values at $\psi = 0$ and $\psi = \pi$. Furthermore, the convergence to the steady state is very fast since the linearization of (4) for small enough velocities is $m_u \dot{u} + |\mathcal{X}_u| u = F_p(a_p)$, thus $u^*(t)$ converges exponentially to u_e^\pm with rate $\frac{|\mathcal{X}_u|}{m_u}$. Therefore, $u^*(\psi)$ converges exponentially fast to u_e^\pm with, at least, the rate $\frac{|\mathcal{X}_u|}{r_{min} m_u}$, which is very large for small enough a_0 . The same applies to $r^*(t)$, thus $\frac{u^*(\psi)}{r^*(\psi)}$ could be replaced in the integral by its steady state value $\frac{u_e^\pm}{r_e^\pm}$:

$$\begin{aligned}\bar{x} &\approx \frac{1}{T} \int_0^{2\pi} \frac{v^*(\psi)}{r^*(\psi)} \sin(\psi) d\psi \\ &\approx \frac{1}{T} \int_0^\pi \frac{v_e^+}{r_e^+} \sin(\psi) d\psi + \frac{1}{T} \int_\pi^{2\pi} \frac{v_e^-}{r_e^-} \sin(\psi) d\psi \\ &= \frac{2}{T} \left(\frac{v_e^+}{r_e^+} - \frac{v_e^-}{r_e^-} \right) \approx -\frac{8Km_u}{T |\mathcal{Y}_v \mathcal{X}_u|} a_0 \Delta a \neq 0\end{aligned}$$

The same reasoning applies to \bar{y} in (21), then, $\bar{y} \neq 0$, and $[V_{xf}, V_{yf}] \neq 0$. \square

Remark 1: Demonstration of Lemma 5 is complex because the control action (11) is discontinuous and it switches depending on the state of the system. Hence, it is not easy or straightforward to prove the existence of an attracting limit cycle. However, despite this complex demonstration, it is very important to highlight the existence of such limit cycle and

that the control action (11) provides satisfactory results, being very simple and easy to apply in practice in case of a thruster failure.

Remark 2: Demonstration of Lemma 5 may suggest that in order to achieve exponential convergence to a sustained advance velocity, a very small a_0 and Δa are needed. However, as it will be shown in the simulation results of Section IV, control action (11) provides stable and good behaviour even for large values of a_0 and Δa , with $\Delta a < a_0$. In fact, in a practical situation, it is usually convenient to select Δa as large as possible without loosing stability, and such that $a_0 - \Delta a$ is also large enough. The latter ensures that the vehicle turns at a reasonable rate, the trajectory reaches a good average velocity, and it is able to reject disturbances.

Once the control action (11), which is able to move the vehicle in “some” direction $\Delta\psi$, has been defined, it is straightforward to modify it to move the vehicle along a predefined desired direction ψ_r :

$$a_p = a_0 + \Delta a \cdot \text{sign}(\sin(\psi + \Delta\psi - \psi_r)) \quad (22)$$

where $\Delta\psi$ is the direction of the average velocity when (11) is applied, i.e. $\Delta\psi = \text{atan2}(V_{yf}, V_{xf})$.

Therefore, control law (22) switches when $\psi = \psi_r - \Delta\psi + 2n\pi$ and $\psi = \psi_r - \Delta\psi + (2n+1)\pi$, as shown in Figure 4, and the vehicle moves in direction ψ_r instead of moving in direction $\Delta\psi$ with respect to the X-axis. Doing this way, the trajectory obtained with (22) is rotated an angle $\psi_r - \Delta\psi$ with respect to the trajectory obtained with (11), and the final average velocity points towards $\Delta\psi + \psi_r - \Delta\psi = \psi_r$.

Theorem 1: Consider system (1)-(6) and control action (22), then a_0 , Δa and $\Delta\psi$ can be chosen such that the average speed of the vehicle converges exponentially to a constant speed $V_f > 0$ in the direction of ψ_r .

Proof: Consider the following change of coordinates, which consists of a rotation of the angle $\rho = \Delta\psi - \psi_r$ of the inertial coordinate frame:

$$\begin{aligned}x' &= \cos(\rho)x - \sin(\rho)y \\ y' &= \sin(\rho)x + \cos(\rho)y \\ \psi' &= \psi + \rho\end{aligned}$$

Differentiating the above equations with respect to time and combining them with (1)-(3), it yields

$$\begin{aligned}\dot{x}' &= u \cos(\psi') - v \sin(\psi') \\ \dot{y}' &= u \sin(\psi') + v \cos(\psi') \\ \dot{\psi}' &= r\end{aligned}$$

Then, the dynamic equations (4-6) of the system are invariant under the rotation since they do not depend on the angle ψ but only on its derivative, which remains unchanged. The control action now is $a_p = a_0 + \Delta a \cdot \text{sign}(\sin(\psi' - \rho + \Delta\psi - \psi_r)) = a_0 + \Delta a \cdot \text{sign}(\sin(\psi'))$. Thus, these are the conditions of Lemma 5 and $[\bar{x}', \bar{y}]^T \rightarrow [V_{xf}, V_{yf}]^T = V_f [\cos(\Delta\psi), \sin(\Delta\psi)]$, where $V_f = \sqrt{V_{xf}^2 + V_{yf}^2}$.

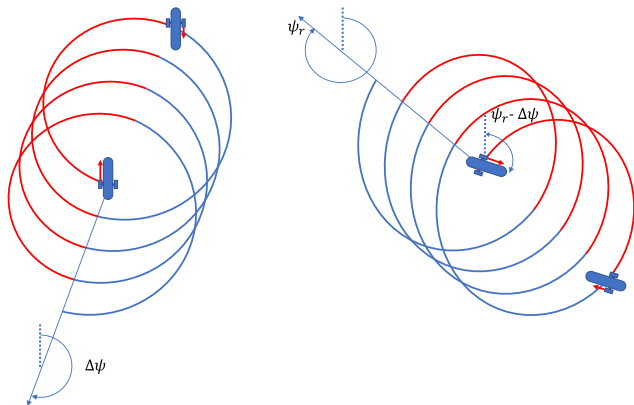


FIGURE 4. Comparison of controllers (11) (left) and (22) (right).

Finally, returning to the original inertial coordinate frame:

$$\begin{aligned} [\bar{x}, \bar{y}]^T &\rightarrow V_f [\cos(-\rho) \cos(\Delta\psi) - \sin(-\rho) \sin(\Delta\psi), \\ &\quad \sin(-\rho) \sin(\Delta\psi) + \cos(-\rho) \cos(\Delta\psi)]^T \\ &= V_f [\cos(\Delta\psi - \rho), \sin(\Delta\psi - \rho)]^T \\ &= V_f [\cos(\psi_r), \sin(\psi_r)]^T \end{aligned}$$

Which concludes the proof. \square

Remark 3: Computing $\Delta\psi$ from its definition in terms of the average speeds (20)-(21) is a complex task. However, it can be computed (or measured experimentally) by simply applying the control action (11) in simulation (or in a real test) during enough time to remove the transient, and then, computing it directly from the average speeds as shown in Figure 4. Furthermore, this means that control law (22) can be applied even if a precise model of the vehicle is not available by directly measuring $\Delta\psi$ with a simple experiment.

B. POSITION CONTROL

Once the average velocity of the vehicle can be controlled, a control law that allows the vehicle to reach the neighbourhood of a desired reference position $\mathbf{X}_r = [x_r, y_r]^T$ must be defined. The direction of the vector that goes from the vehicle position $\mathbf{X} = [x, y]^T$ to the target point \mathbf{X}_r is used as reference for the orientation of the average advance velocity:

$$\psi_r(x, y) = \text{atan2}(y_r - y, x_r - x) \quad (23)$$

$$a_p = a_0 + \Delta a \cdot \text{sign}(\sin(\psi + \Delta\psi - \psi_r(x, y))) \quad (24)$$

This strategy is depicted in Figure 5. While the vehicle makes turns, the control action will switch when $\psi = n\pi + \psi_r(x, y) - \Delta\psi$ with $n = 1, 2, \dots$, and the trajectory will approach the target point. To prove the previous statement, **it is important to notice that ψ_r changes as the vehicle moves**. In fact, ψ_r is, in general, different for each control switch, so Theorem 1 cannot be applied directly. This difficulty is addressed by Lemma 6, which essentially ensures that, for bounded variation of ψ_r over two consecutive switches of the control law, the movement of the vehicle is only slightly disturbed, and the disturbance grows linearly with the variation of ψ_r .

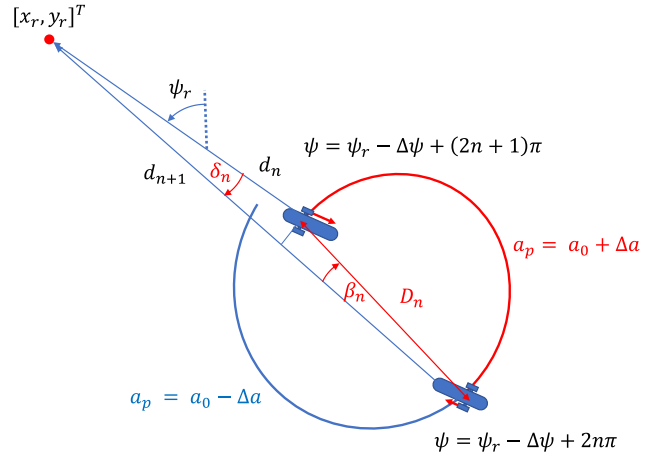


FIGURE 5. Behaviour of the control law (23)-(24) and main variables involved in the process.

Lemma 6: Consider the system (1)-(6) under the piecewise constant control action $a_p = a_0 + \Delta a \cdot \text{sign}(\sin(\psi(t) + \Delta\psi - \psi_r(t)))$, where a_0 and Δa are selected according to Theorem 1. Define t_n as the times where the control action switches, i.e. when $\psi(t_n) + \Delta\psi - \psi_r(t_n) = n\pi$. Define also $\delta_n = \psi_r(t_{n+1}) - \psi_r(t_n)$ as the difference between ψ_r in two consecutive switches of the control law, and also $[\Delta x_n, \Delta y_n]^T = [x(t_{n+2}) - x(t_n), y(t_{n+2}) - y(t_n)]^T$ as the distance covered after two consecutive control switches.

Assume that infinitely many switching times t_n , $n = 1, 2, \dots, \infty$ exist, and that δ_n is bounded $0 \leq |\delta_n| < \delta_m$ for some positive constant δ_m . Then, $[\Delta x_n, \Delta y_n]^T$ converges exponentially to $[\Delta x_n, \Delta y_n]^T = T V_f [\cos(\psi_r(t)), \sin(\psi_r(t))]^T + \gamma(t)$ as $n \rightarrow \infty$, where T is the period of the unperturbed trajectory ($\delta_m = 0$) and $\gamma(t)$ is a bounded function such that, before some transient time t_s , $\|\gamma(t)\| \leq c_9 \delta_m$ for some positive constant c_9 .

Proof: Consider first the system (1)-(6) under the control action $a_p = a_0 + \Delta a \cdot \text{sign}(\sin(\psi(t) + g(t)))$ where $g(t)$ is an arbitrary function of time such that $|g(t_n)| \leq g_m$ for some positive constant g_m . Following the same reasoning of Lemma 5 and considering the new term $g(t_n)$, (15) now yields:

$$\psi(t_{n+1}) - \psi(t_n) = \int_{t_n}^{t_{n+1}} r(s) ds = \pi + g(t_{n+1}) - g(t_n)$$

as $\psi(t)$ must go from $\psi(t_n) = n\pi - g(t_n)$ to $\psi(t_{n+1}) = (n+1)\pi - g(t_{n+1})$ for the control action to switch. Therefore, the trajectory of the velocity can be seen as a perturbed version of the fixed point trajectory \mathbf{v}^* of Lemma 5. It is important to remark that the only effect of $g(t)$ is that it modifies the times at which the control action switches, so only $g(t_n)$, $n = 1, 2, \dots$, are important for the analysis. Further, if $\delta_m = 0$, the term $g(t)$ will have no effect, and the trajectory converges to the periodic (with period T) solution of Lemma 5.

Consider the fixed point velocity \mathbf{v}_n^* and the perturbed velocity \mathbf{v}_n starting at the same time t_n (i.e. $t_n = t_n^*$). Then, the subsequent switching times will be different. This difference

can be obtained by considering the additional term $g(t_{n+1}) - g(t_n)$ into (17):

$$\begin{aligned} |t_{n+1} - t_{n+1}^*|r_{min} &\leq \frac{c_1}{c_2} \|\mathbf{v}_n - \mathbf{v}_n^*\| + |g(t_{n+1}) - g(t_n)| \\ &\leq \frac{c_1}{c_2} \|\mathbf{v}_n - \mathbf{v}_n^*\| + \delta_m \end{aligned} \quad (25)$$

Including this new term δ_m on (18) yields

$$\|\mathbf{v}_{n+1} - \mathbf{v}_{n+1}^*\| \leq \alpha_1 \|\mathbf{v}_n - \mathbf{v}_n^*\| + \frac{c_4 c_8 \Delta a \delta_m}{r_{min}}$$

Then, a modified version of (19) can be computed:

$$\|\mathbf{v}_{n+2} - \mathbf{v}_{n+2}^*\| \leq \alpha \|\mathbf{v}_n - \mathbf{v}_n^*\| + c_{10} \Delta a \delta_m$$

where $c_{10} = \left(1 + c_1 e^{-c_2 \Delta t_{n+1}} + \frac{2c_1 c_4 \Delta a}{c_2 r_{min}}\right) \frac{2c_4 c_8}{r_{min}}$, and after k cycles:

$$\begin{aligned} \|\mathbf{v}_{n+2k} - \mathbf{v}_{n+2k}^*\| &\leq \alpha \|\mathbf{v}_{n+2(k-1)} - \mathbf{v}_{n+2(k-1)}^*\| + c_{10} \Delta a \delta_m \\ &\leq \alpha^2 \|\mathbf{v}_{n+2(k-2)} - \mathbf{v}_{n+2(k-2)}^*\| + (\alpha^2 + 1)c_{10} \Delta a \delta_m \\ &\leq \alpha^3 \|\mathbf{v}_{n+2(k-3)} - \mathbf{v}_{n+2(k-3)}^*\| + (\alpha^2 + \alpha + 1)c_{10} \Delta a \delta_m \\ &\dots \\ &\leq \alpha^k \|\mathbf{v}_n - \mathbf{v}_n^*\| + \sum_{i=0}^{k-1} \alpha^i c_{10} \Delta a \delta_m \\ &\leq \alpha^k \|\mathbf{v}_n - \mathbf{v}_n^*\| + \sum_{i=0}^{\infty} \alpha^i c_{10} \Delta a \delta_m \\ &\leq \alpha^k \|\mathbf{v}_n - \mathbf{v}_n^*\| + \frac{c_{10}}{1-\alpha} \Delta a \delta_m \end{aligned}$$

Therefore, the difference between \mathbf{v}_n and \mathbf{v}_n^* is globally ultimately bounded, its norm converges exponentially fast to the bound, and there exists a k large enough such that the first term becomes smaller than $\frac{c_{10}}{1-\alpha} \Delta a \delta_m$. Naming this time t_s and due to the continuity of the solutions on the finite interval, then $\|\mathbf{v}(t) - \mathbf{v}^*(t)\| \leq c_{10} \Delta a \delta_m$ for $t_s \leq t_n \leq t \leq t_n + T$, where c_{10} is a positive constant.

The displacement $\Delta x_n = x(t_{n+2}) - x(t_n)$ over the X-coordinate during this time interval is given by:

$$\begin{aligned} \Delta x_n &= \int_{t_n}^{t_{n+2}} (u \cos(\psi) - v \sin(\psi)) dt \\ &= \int_{t_n}^{t_n+T} (u \cos(\psi) - v \sin(\psi)) dt \\ &\quad + \int_{t_n+T}^{t_{n+2}} (u \cos(\psi) - v \sin(\psi)) dt \end{aligned} \quad (26)$$

Rewriting the first term as $u \cos(\psi) = u^* \cos(\Delta\psi) + u^*(\cos(\psi) - \cos(\Delta\psi)) + (u - u^*) \cos(\psi)$, we may write:

$$\begin{aligned} |u \cos(\psi) - u^* \cos(\Delta\psi)| &\leq |u^*| |\cos(\psi) - \cos(\Delta\psi)| + |(u - u^*)| |\cos(\psi)| \\ &\leq V_{max} |\cos(\psi) - \cos(\Delta\psi)| + |(u - u^*)| \\ &\leq (V_{max} + 1) \|\mathbf{v} - \mathbf{v}^*\| \leq (V_{max} + 1) c_{10} \Delta a \delta_m \end{aligned}$$

where V_{max} is the maximum advance speed that the vehicle can reach. The same argument applies for the second term $v \sin(\psi)$ of (26).

Consider now the difference between the periods of the perturbed trajectory and the unperturbed one, i.e., $t_{n+2} - (t_n + T) = (t_{n+2} - t_n) - T$. Then, considering that $T = t_{n+2}^* - t_n^* = t_{n+2}^* - t_{n+1}^* + t_{n+1}^* - t_n^*$, and doing the same with $t_{n+2} - t_n$, yields:

$$\begin{aligned} |t_{n+2} - t_n - T| &= |t_{n+2} - t_{n+1} + t_{n+1} - t_n \\ &\quad - (t_{n+2}^* - t_{n+1}^* + t_{n+1}^* - t_n^*)| \\ &\leq |t_{n+2} - t_{n+1} - (t_{n+2}^* - t_{n+1}^*)| \\ &\quad + |t_{n+1} - t_n - (t_{n+1}^* - t_n^*)| \\ &\leq \frac{c_1}{r_{min} c_2} \|\mathbf{v}_{n+1} - \mathbf{v}_{n+1}^*\| + \frac{\delta_m}{r_{min}} \\ &\quad + \frac{c_1}{r_{min} c_2} \|\mathbf{v}_n - \mathbf{v}_n^*\| + \frac{\delta_m}{r_{min}} \\ &\leq \frac{2c_1 c_8}{r_{min} c_2 (1-\alpha)} \Delta a \delta_m + \frac{2\delta_m}{r_{min}} \\ &= \frac{2c_1 c_8 \Delta a + 2c_2 (1-\alpha)}{r_{min} c_2 (1-\alpha)} \delta_m \end{aligned} \quad (27)$$

Since the second term of the right hand side of (27) is $|t_{n+1} - t_n - (t_{n+1}^* - t_n^*)| = |t_{n+1} - t_{n+1}^*|$, and the first term is the translation of the second one a step further ($n \rightarrow n+1$), both terms can be bounded using (25).

In addition, the first integral in (26) applied to the fixed point trajectory \mathbf{v}^* is given by TV_{xf} (see (20)), so Δx_n may be written as $\Delta x_n = TV_{xf} + \xi_x$. Then:

$$\begin{aligned} |\xi_x| &= |\Delta x_n - TV_{xf}| \\ &\leq \int_{t_n}^{t_n+T} (|u \cos(\psi) - u^* \cos(\Delta\psi)| \\ &\quad + |v \sin(\psi) - v^* \sin(\Delta\psi)|) dt \\ &\quad + \left| \int_{t_n+T}^{t_{n+2}} (u \cos(\psi) - v \sin(\psi)) dt \right| \\ &\leq 2T(V_{max} + 1)c_{10}\Delta a \delta_m \\ &\quad + V_{max} \frac{2c_1 c_8 \Delta a + 2c_2 (1-\alpha)}{r_{min} c_2 (1-\alpha)} \delta_m = c_9 \delta_m \end{aligned} \quad (28)$$

where each term of the first integral in (28) is bounded by $(V_{max} + 1)c_{10}\Delta a \delta_m$. The term of the second integral is bounded because $|u \cos(\psi) - v \sin(\psi)| \leq V_{max}$, and the time differences are bounded by (27).

The same applies to the displacement over the Y-axis, which yields $\Delta y_n = TV_{yf} + \xi_y$, where $|\xi_y| \leq c_9 \delta_m$.

Hence, coming back to the original control law $a_p = a_0 + \Delta a \cdot \text{sign}(\sin(\psi_r(t) + \Delta\psi) - \psi_r(t))$ and applying the same argument of Theorem 1, we obtain:

$$\begin{aligned} [\Delta x_n, \Delta y_n]^T &\rightarrow TV_f [\cos(\psi_r(t_n)), \sin(\psi_r(t_n))]^T \\ &\quad + [\xi_x \cos(\psi_r(t_n)), \xi_y \sin(\psi_r(t_n))]^T \\ &= TV_f [\cos(\psi_r(t_n)), \sin(\psi_r(t_n))]^T + \gamma(t) \end{aligned}$$

Finally $\|\gamma(t)\| = \sqrt{\cos(\psi_r)^2 \xi_x^2 + \sin(\psi_r)^2 \xi_y^2} \leq c_9 \delta_m$ for $t > t_s$. \square

With Lemma 6 at hand, the main result of the present work is presented:

Theorem 2: Consider system (1)-(6) and control action (23)-(24), then a_0 , Δa and $\Delta \psi$ can be chosen such that the distance to the target point $[x_r, y_r]$ is globally uniformly ultimately bounded.

Proof: The vehicle turns monotonically infinitely as time passes because the angular speed of the vehicle is lower bounded by r_{min} . Define $\mathbf{X}_n = [x_n, y_n]^T$ as the position of the vehicle at time t_n , $\mathbf{X}_r = [x_r, y_r]^T$ as the target point, and $d_n = \|\mathbf{X}_n - \mathbf{X}_r\|$ as the distance from the vehicle to the target point at t_n , as shown in Figure 5.

Then, there are two possibilities:

1) There exists a time t_{end} such that the control law stops switching for $t > t_{end}$ and remains constant. In this case the trajectory converges to a circumference, as seen in Section III-A. Furthermore, since the control law must remain constant, then $\sin(\psi + \Delta\psi - \psi_r(x, y))$ is bounded and different from zero. This can only happen if the trajectory encircles the target point. Notice also that the diameter of the trajectory over one turn (i.e the maximum distance between two points of the trajectory over one revolution) is bounded since the vehicle completes a turn in at most $\frac{2\pi}{r_{min}}$ seconds, and, during this time, it can travel a maximum distance of $D_{max} = \frac{2\pi V_{max}}{r_{min}}$. Therefore, the vehicle's trajectory encircles \mathbf{X}_r , the diameter is bounded by D_{max} , and thus, the distance from the vehicle to the target point is globally finally bounded by D_{max} .

2) There exists an infinite sequence of times t_n , $n = 1, 2, \dots$, at which the control law switches. Define $d_n = d(t_n)$ as the distance from the vehicle to the target point at switching time t_n , $D_n = \|\mathbf{X}(t_{n+1}) - \mathbf{X}(t_n)\|$ as the distance between two consecutive switching times, $\delta_n = \psi_r(t_{n+1}) - \psi_r(t_n)$ as the difference between the orientation angles to the target point at two consecutive switching times (see Lemma 6), and β_n as the angle shown in Figure 5.

The triangle formed by d_n , d_{n+1} and D_n in Figure 5 is such that $D_n \sin(|\beta_n|) = d_n \sin(|\delta_n|)$, and as $D_n \leq D_{max}$, then:

$$\sin(|\delta_n|) \leq \frac{D_{max}}{d_n}.$$

The position \mathbf{X}_n of the vehicle at time t_n is:

$$\mathbf{X}_n = \mathbf{X}_r - [d_n \sin(\psi_r), d_n \cos(\psi_r)]^T$$

Then, define d_{lim} as follows:

$$d_{lim} = \max \left(TV_f, \frac{D_{max}}{\sin \left(\frac{\alpha TV_f}{c_9} \right)} \right)$$

where $0 < \alpha < 1$ is the constant from (19), which can be chosen such that $\sin \left(\frac{\alpha TV_f}{c_9} \right)$ is not zero. Then if $d_n \geq d_{lim}$, then $d_n \geq TV_f$, $d_n \geq D_{max}$ and $\alpha TV_f \geq c_9 \cdot \arcsin \left(\frac{D_{max}}{d_n} \right)$, so:

$$d_n \geq d_{lim} \rightarrow \sin(|\delta_n|) \leq \frac{D_{max}}{d_n}.$$

Then,

$$|\delta_n| \leq \arcsin \left(\frac{D_{max}}{d_n} \right) \leq \frac{\alpha TV_f}{c_9}.$$

If $d_n \geq d_{lim}$ the conditions of Lemma 6 applies with $\delta_m = \frac{\alpha TV_f}{c_9}$, and, for large enough n , the new position \mathbf{X}_{n+1} at time $t_{n+1} > t_s$ becomes:

$$\begin{aligned} \mathbf{X}_{n+1} &= \mathbf{X}_r - [d_n \sin(\psi_r), d_n \cos(\psi_r)]^T \\ &\quad + TV_f [\cos(\psi_r), \sin(\psi_r)]^T + \boldsymbol{\gamma}(t) \\ &= \mathbf{X}_r + [(TV_f - d_n) \sin(\psi_r), (TV_f - d_n) \cos(\psi_r)]^T \\ &\quad + \boldsymbol{\gamma}(t) \end{aligned}$$

where $\|\boldsymbol{\gamma}(t)\| \leq c_9 \delta_m = c_9 \cdot \frac{\alpha TV_f}{c_9} = \alpha TV_f$. Therefore, in this case, the new distance d_{n+1} after one turn is:

$$\begin{aligned} d_{n+1} &= \|\mathbf{X}_{n+1} - \mathbf{X}_r\| \\ &\leq |(TV_f - d_n)| \|[\sin(\psi_r), \cos(\psi_r)]^T\| + \|\boldsymbol{\gamma}(t)\| \\ &\leq |d_n - TV_f| + \|\boldsymbol{\gamma}(t)\| \\ &\leq d_n - TV_f + \alpha TV_f = d_n - (1 - \alpha)TV_f < d_n \end{aligned}$$

The last equation implies that the distance d_n decreases monotonically until it reaches d_{lim} , and, once $d_n < d_{lim}$ the distance can grow. However, if $d_n > d_{lim}$, then the conditions of Lemma 6 apply again and before some time t_s the distance will decrease. Therefore, d_n is globally finitely bounded by $d_{lim} + V_{max} t_s$. Furthermore, the distance from the vehicle to the target point is $d = \|\mathbf{X} - \mathbf{X}_r\| \leq \|\mathbf{X} - \mathbf{X}_n\| + \|\mathbf{X}_n - \mathbf{X}_r\| \leq D_{max} + d_{lim} + V_{max} t_s$, which is GUUB. \square

Remark 4: It is important to highlight again the simplicity and elegance of the control law (23)-(24), which can be obscured by the complexity of the proofs. In addition, it is essential to keep in mind that this control law is able to drive the vehicle to the neighbourhood of any desired target point by only using one motor and two control values $a_p = a_0 \pm \Delta a$, which is the absolute bare minimum to be able to control the vehicle.

IV. RESULTS

The well performance and behaviour of the control law (23)-(24) is now demonstrated through several simulation examples under different conditions and situations, showing how it is possible to drive the vehicle to the desired target point with only one thruster and a limited set of inputs. The vehicle parameters used for the simulations are shown in Table 2. These parameters have been obtained experimentally from previous tests carried out with the MEDUSA-AUV shown in Figure 1.

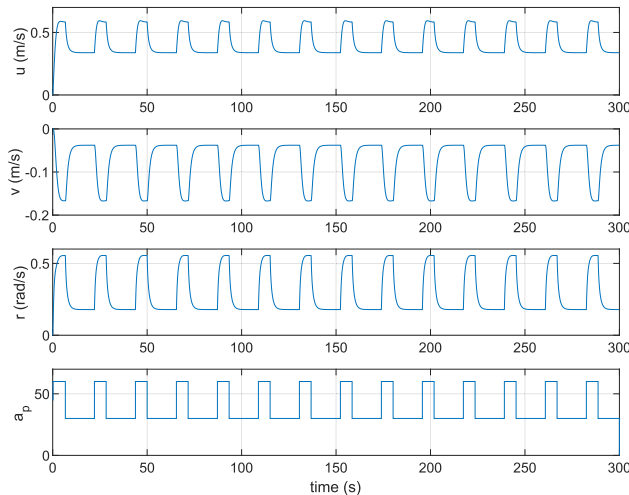
A. EXAMPLE 1: MOVEMENT IN A ARBITRARY DIRECTION

In this first example, the aim is to show how, using control action (11), the vehicle moves towards a direction with a non-zero average advance velocity.

For the example, control (11) is applied considering $a_0 = 45$, and $\Delta a = 15$. Thus, the two control actions applied to the vehicle are $a_p = a_0 - \Delta a = 30$ and $a_p = a_0 + \Delta a = 60$,

TABLE 2. Parameters of the AUV model used in simulations.

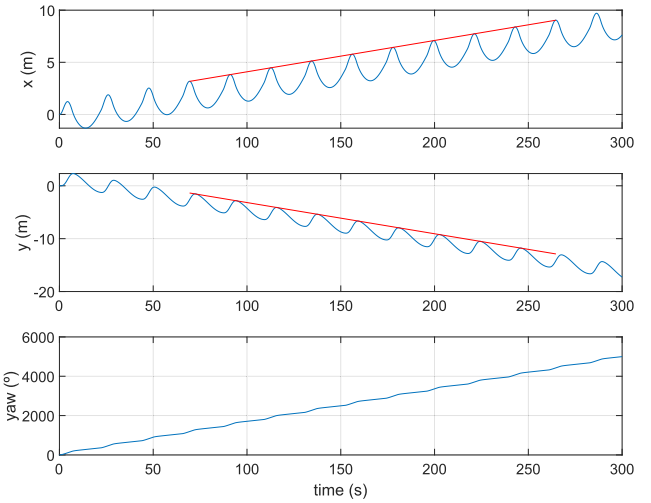
L	0.25 m
m_u	37 kg
m_v	47 kg
m_r	$4.64 \text{ kg} \cdot \text{m}^2$
\mathcal{K}	$3.6 \cdot 10^{-3} \text{ N}$
\mathcal{X}_u	$-0.2 \text{ kg} \cdot \text{s}^{-1}$
\mathcal{Y}_v	$-55.1 \text{ kg} \cdot \text{s}^{-1}$
\mathcal{N}_r	$-4.14 \text{ kg} \cdot \text{m}^2 \cdot \text{s}^{-1}$
$\mathcal{X}_{ u }$	$-25 \text{ kg} \cdot \text{m}^{-1}$
$\mathcal{Y}_{ v }$	$-101.3 \text{ kg} \cdot \text{m}^{-1}$
$\mathcal{N}_{ r }$	$-6.23 \text{ kg} \cdot \text{m}^2$

**FIGURE 6.** From top to bottom: Surge speed, sway speed, yaw rate and control action under control law (11).

where a_p is normalised to the range $[-100, 100]$. The vehicle starts from point $\mathbf{X}_0 = [0, 0]$ and zero initial conditions, i.e., $\psi_0 = 0$ and $\mathbf{v}_0 = [u_0, v_0, r_0]^T = [0, 0, 0]^T$.

Figure 6 shows how, after a transitory of approximately 10 seconds, the speeds of the system reach very fast a limit cycle of sustained oscillations, as Lemma 5 claims. Therefore, by keeping this switching control law constant over the appropriate time window, the vehicle will advance in a given direction. Notice how the speeds change according to the switching of the control action a_p . The asymmetric switching times, which are consequence of the different angular speeds of each interval of the control law, allow the vehicle to follow, in average sense, a straight line. This fact can be checked in the position and orientation of the vehicle under control (11) depicted in Figure 7 for a time window of 300 seconds. Notice that from this figure it is possible to measure the average velocity after the transient. The average velocity components are $V_{xf} = 3\text{cm}/\text{s}$, $V_{yf} = -5.9\text{cm}/\text{s}$, and thus $V_f = 6.62\text{cm}/\text{s}$. The red lines in the figure show how the estimated average velocity is computed. Moreover, it is possible to compute the angle $\Delta\psi = -63^\circ$ that defines the direction towards which the vehicle moves.

The whole trajectory followed by the AUV during 300 seconds is depicted in Figure 8, from which it is also possible to determine $\Delta\psi$.

**FIGURE 7.** Position and orientation of the vehicle under control law (11).**TABLE 3.** Initial conditions for trajectories of Example 2 and Example 3.

\mathbf{X}_0 [m,m]	\mathbf{v}_0 [m/s, m/s, rad/s]	ψ_0 [rad]
[-20, -20] (blue)	[0,0,0]	0
[-10, 20] (red)	[0,0,0]	$\pi/2$
[20, 20] (green)	[1,1,1]	0
[20, -10] (yellow)	[0,0,0]	$-\pi/2$

B. EXAMPLE 2: GUIDANCE TO A SELECTED RECOVERY POINT

In this second example, it is shown how the vehicle can be driven from any starting point to a desired target point, which is the origin of the coordinate frame for the example at hand. The same parameters of Example 1 for the control law are used. Thus, $\Delta\psi = -63^\circ$ is already known and control action (23)-(24) can be applied.

Figure 9 shows the trajectories followed by the AUV starting from 4 different initial conditions. These initial conditions \mathbf{X}_0 , $\mathbf{v}_0 = [u_0, v_0, t_0]^T$ and ψ_0 are shown in Table 3. As mentioned, for all the cases the reference target point is $\mathbf{X}_r = [0, 0]$. Figure 9 shows that, starting from any initial condition, the trajectories of the AUV converge to a neighbourhood of the origin following a “straight” (in an average sense) path and eventually the trajectory encircles the reference point and the control law stops switching.

C. EXAMPLE 3: ROBUSTNESS TO UNCERTAINTY ON THE ANGLE $\Delta\psi$

In this third example, it is shown that an accurate estimation of the parameters, such as $\Delta\psi$, are not needed for a correct behaviour of the control law.

The robustness of the controller to changes in the parameters can be easily illustrated by selecting the angle $\Delta\psi$ as a very rough estimate of its true value. In this sense, and considering the same initial conditions of Example 2 shown in Table 3, the angle $\hat{\Delta}\psi = -90^\circ$ is selected, almost 30° far from the optimal one, which was $\Delta\psi = -63^\circ$.

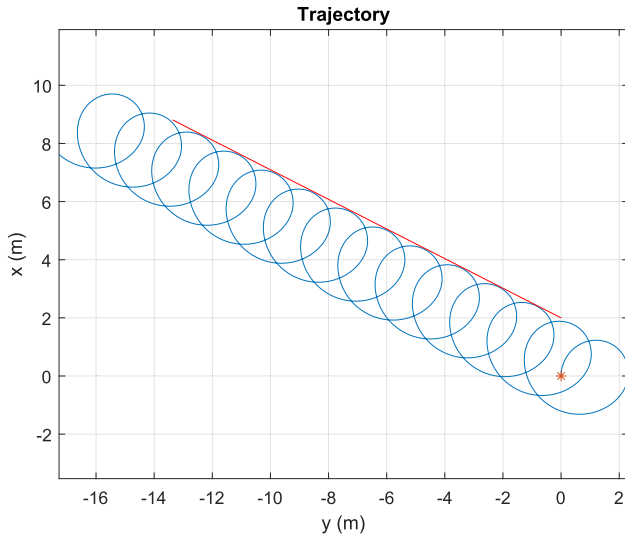


FIGURE 8. Trajectory of the AUV under control law (11) during the first 300 seconds.

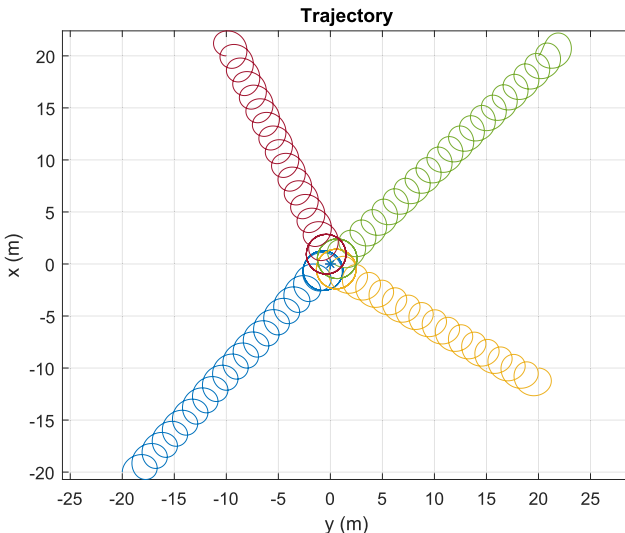


FIGURE 9. Trajectories of the AUV under control law (23)-(24) starting from different initial conditions. The initial conditions are shown in Table 3.

Figure 10 shows that, although the trajectories are not as “straight” as in Example 2, they finally encircle the reference point.

D. EXAMPLE 4: ROBUSTNESS TO CHANGES IN THE CONTROL LAW PARAMETERS

Theoretical results could suggest that, in order to obtain convergence to a neighbourhood of the target point, a careful selection of the control parameters is needed. On the contrary, the control is very robust to changes in all the control parameters. To illustrate it, Figure 11 depicts the trajectories of the system starting from initial conditions $\mathbf{X}_0 = [-20, 20]$, $\mathbf{v}_0 = [0, 0, 0]^T$, $\psi_0 = 0$, and for $a_0 = 20, 50, 66$ and $\Delta a = \frac{a_0}{2}$, so that $\Delta a \leq a_0$. These values cover the full

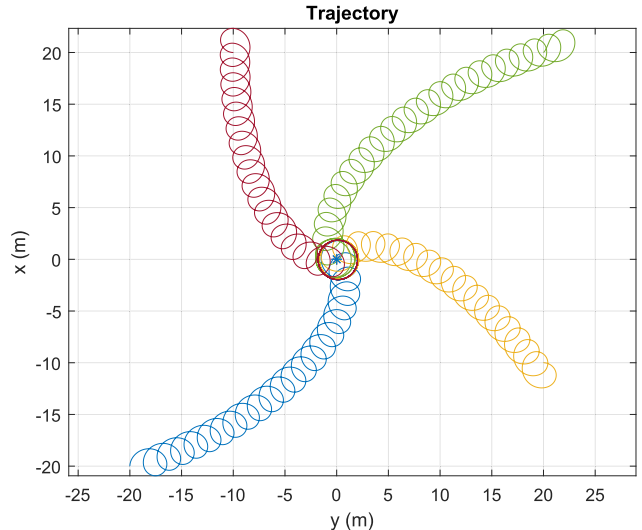


FIGURE 10. Trajectories of the AUV under uncertainty on the value of $\Delta\psi$.

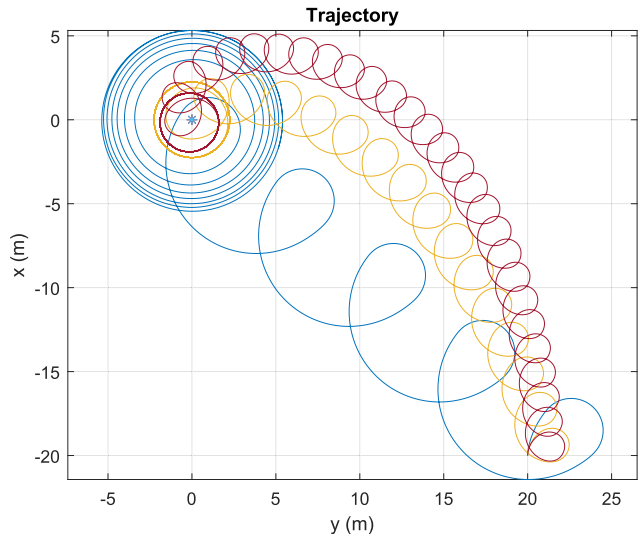


FIGURE 11. Trajectories of the AUV for $a_0 = 20, 50, 66$ (blue, yellow and red respectively), $\Delta a = \frac{a_0}{2}$ and $\hat{\Delta\psi} = -90^\circ$.

range of the actuator since $a_p = a_0 \pm \Delta a$ ranges from 10% to 99% of thrust. In addition, for all cases $\hat{\Delta\psi} = -90^\circ$ was selected. This selected value for $\Delta\psi$ is not optimal for any of the a_0 and Δa mentioned above, but it is enough so that the vehicle does not take so much time to reach the target point. As Figure 11 shows, the control law works well in practice even for not optimal parameters, and in all cases the trajectories finally encircle the target point. Notice that $a_0 = 20$ is a very bad selection of the control parameters, as the blue trajectory shows. It requires more time to reach the final trajectory that encircles the target point, and also the distance at which the vehicle keeps turning is larger compared with other controllers. However, despite this bad parameter selection, the vehicle can reach the neighbourhood of the target point and keep moving in a stable circular trajectory.

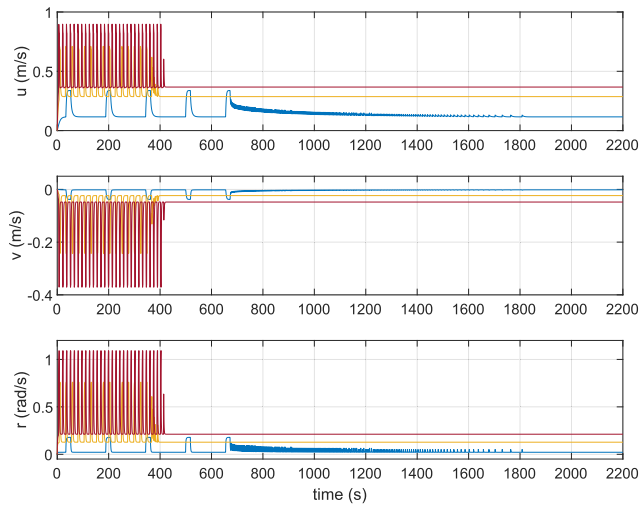


FIGURE 12. Speeds of the AUV for $a_0 = 20, 50, 66$ (blue, yellow and red respectively), $\Delta\alpha = \frac{a_0}{2}$ and $\Delta\dot{\psi} = -90^\circ$.

To clearly see the behaviour of each of the controllers for their corresponding values of a_0 , Figure 12 shows the speeds of the AUV. Notice that for $a_0 = 66$ the trajectory encircles the target point at $t = 415s$ and the control law stops switching. For $a_0 = 50$ the trajectory encircles the target point at $t = 367s$ but it has a transitory before control law stops switching at $t = 392s$. Finally, for $a_0 = 20$ the trajectory takes more time to reach the target point, which is encircled at $t = 671s$, and the transitory is also longer since it gets trapped in a slowly diverging (but ultimately bounded) trajectory such that $\sin(\psi + \Delta\psi - \psi_r) \approx 0$. This condition is pathological (and a consequence of a very bad choice of the control parameters) because it causes fast switching of the controller during the time interval $672s \leq t \leq 1812s$ until it eventually stops and the AUV keeps moving on a circular trajectory around the target point. This example illustrates that the behaviour of the vehicle, once the trajectory is close to the target point, could be complex if the parameters selection is done arbitrarily, randomly or wrongly.

E. EXAMPLE 5: ROBUSTNESS TO DISTURBANCES

In this final example, the robustness of the controller to external disturbances is studied. In order to do so a constant current V_c is introduced in the direction of the Y -axis by replacing (2) by $\dot{y} = u \sin(\psi) + v \cos(\psi) + V_c$. Since the average velocity that the vehicle can reach is limited (and usually small compared with the velocity that can be reached in normal operation) the current speed must be less than V_f so that the AUV can overcome it. Thus, the controller is tested for different current speeds, $V_c = 0.1V_f, 0.4V_f, 0.7V_f$ and $0.9V_f$, with the AUV starting from initial conditions $\mathbf{X}_0 = [-20, 20]$, $\mathbf{v}_0 = [0, 0, 0]^T$ and $\psi_0 = 0$. Figure 13 shows the good performance that is obtained for moderate disturbances (up to 70% of the maximum speed of the AUV). However, when the disturbance is close to V_f , the performance degrades

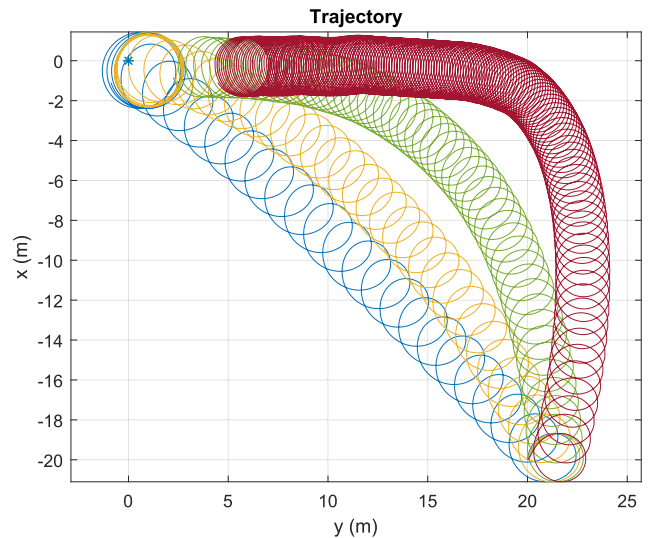


FIGURE 13. Trajectories of the AUV under constant disturbances. A constant current in the Y-Axis with speed $V_c = 0.1V_f, 0.4V_f, 0.7V_f$ and $0.9V_f$ (blue, yellow, green and red, respectively) is considered.

rapidly, as expected. In fact, as the disturbance increases, the average velocity of the vehicle towards the target point decreases. In the limit case that $V_c = V_f$ the vehicle is not able to even approach the target point.

V. CONCLUSION

In this work a fault-tolerant control to be used in emergency situations has been designed. This control law allows to drive the vehicle to a selected target point, i.e., a safety recovery point, by carrying out a homing operation with a single operative thruster controlled by discrete inputs. The resultant trajectory of the vehicle describes a spiral-like path due to the use of a single thruster. However, by adequately controlling the switching times of the control law, it is possible to drive the vehicle, in average, towards the desired direction and keep it in the neighbourhood of the target point. The stability and convergence of the control law have been analytically demonstrated, and its good performance has been shown in several examples. In these examples, it has been demonstrated how the control law is able to drive and keep the AUV within the neighbourhood of the desired target point even when there is uncertainty in the parameters, when the parameters are not optimal, and under constant disturbances.

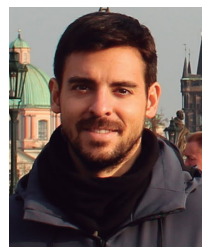
Future work will aim to test the well performance of the control law in an experimental setup and to develop new controllers for the same faulty situation in which only one thruster is available, but trying to optimize different parameters, such as energy consumption, time, speed, etc. This will allow to compare different controllers for similar situations, and to be able to determine if, in a situation of emergency in which only one thruster keeps working, it is better to use an optimized controller (for a given parameter) or a simple and general controller, as the one proposed in the present paper, is enough and more appropriate for this urgent action.

REFERENCES

- [1] R. Ghacheloo, A. P. Aguiar, A. Pascoal, C. Silvestre, I. Kaminer, and J. Hespanha, "Coordinated path-following in the presence of communication losses and time delays," *SIAM J. Control Optim.*, vol. 48, no. 1, pp. 234–265, 2009, doi: 10.1137/060678993.
- [2] D. Moreno-Salinas, A. Pascoal, and J. Aranda, "Optimal sensor placement for acoustic underwater target positioning with range-only measurements," *IEEE J. Ocean. Eng.*, vol. 41, no. 3, pp. 620–643, Jul. 2016.
- [3] N. Crasta, D. Moreno-Salinas, A. Pascoal, and J. Aranda, "Multiple autonomous surface vehicle motion planning for cooperative range-based underwater target localization," *Annu. Rev. Control*, vol. 46, pp. 326–342, Oct. 2018. [Online]. Available: <http://www.sciencedirect.com/science/article/pii/S136757881830107X>
- [4] T. K. Podder and N. Sarkar, "Fault-tolerant control of an autonomous underwater vehicle under thruster redundancy," *Robot. Auto. Syst.*, vol. 34, no. 1, pp. 39–52, 2001. [Online]. Available: <http://www.sciencedirect.com/science/article/pii/S0921889000001007>
- [5] G. Antonelli, *A Survey of Fault Detection/Tolerance Strategies for AUVs and ROVs Booktitle=Fault Diagnosis and Fault Tolerance for Mechatronic Systems: Recent Advances*. Berlin, Germany: Springer, 2003, pp. 109–127.
- [6] N. Sarkar, T. K. Podder, and G. Antonelli, "Fault-accommodating thruster force allocation of an AUV considering thruster redundancy and saturation," *IEEE Trans. Robot. Autom.*, vol. 18, no. 2, pp. 223–233, Apr. 2002.
- [7] J. G. Rauber, C. H. F. dos Santos, A. C. B. Chiella, and L. R. H. Motta, "A strategy for thruster fault-tolerant control applied to an AUV," in *Proc. 17th Int. Conf. Methods Models Autom. Robot. (MMAR)*, Aug. 2012, pp. 184–189.
- [8] L. Pugi, B. Allotta, and M. Pagliai, "Redundant and reconfigurable propulsion systems to improve motion capability of underwater vehicles," *Ocean Eng.*, vol. 148, pp. 376–385, Jan. 2018. [Online]. Available: <http://www.sciencedirect.com/science/article/pii/S0029801817307084>
- [9] A. Baldini, L. Ciabattoni, R. Felicetti, F. Ferracuti, A. Freddi, and A. Monteriù, "Dynamic surface fault tolerant control for underwater remotely operated vehicles," *ISA Trans.*, vol. 78, pp. 10–20, 2018, advanced Methods in Control and Signal Processing for Complex Marine Systems. [Online]. Available: <https://www.sciencedirect.com/science/article/pii/S0019057818300806>
- [10] M. Andonian, D. Cazzaro, L. Invernizzi, M. Chyba, and S. Grammatico, "Geometric control for autonomous underwater vehicles: Overcoming a thruster failure," in *Proc. 49th IEEE Conf. Decis. Control (CDC)*, Dec. 2010, pp. 7051–7056.
- [11] M. Leonetti, S. R. Ahmadzadeh, and P. Kormushev, "On-line learning to recover from thruster failures on autonomous underwater vehicles," in *Proc. OCEANS*, Sep. 2013, pp. 1–6.
- [12] S. R. Ahmadzadeh, M. Leonetti, A. Carrera, M. Carreras, P. Kormushev, and D. G. Caldwell, "Online discovery of AUV control policies to overcome thruster failures," in *Proc. IEEE Int. Conf. Robot. Automat. (ICRA)*, May 2014, pp. 6522–6528.
- [13] G. Zhang, S. Chu, X. Jin, and W. Zhang, "Composite neural learning fault-tolerant control for underactuated vehicles with event-triggered input," *IEEE Trans. Cybern.*, vol. 51, no. 5, pp. 2327–2338, May 2021.
- [14] Y. Yang, J. Wang, Z. Wu, and J. Yu, "Fault-tolerant control of a CPG-governed robotic fish," *Engineering*, vol. 4, no. 6, pp. 861–868, Dec. 2018. [Online]. Available: <http://www.sciencedirect.com/science/article/pii/S2095809918301085>
- [15] X.-Z. Jin, G.-H. Yang, X.-H. Chang, and W.-W. Che, "Robust fault-tolerant H_∞ control with adaptive compensation," *Acta Automatica Sinica*, vol. 39, no. 1, pp. 31–42, 2013. [Online]. Available: <https://www.sciencedirect.com/science/article/pii/S187410291360004X>
- [16] J. Xiong, X. H. Chang, J. H. Park, and Z. M. Li, "Nonfragile fault-tolerant control of suspension systems subject to input quantization and actuator fault," *Int. J. Robust Nonlinear Control*, vol. 30, no. 16, pp. 6720–6743, 2020, doi: 10.1002/rnc.5135.
- [17] G. Antonelli, F. Caccavale, C. Sansone, and L. Villani, "Fault diagnosis for AUVs using support vector machines," in *Proc. IEEE Int. Conf. Robot. Automat. (ICRA)*, Apr. 2004, pp. 4486–4491.
- [18] M. Corradini, A. Monteriù, and G. Orlando, "An actuator failure tolerant control scheme for an underwater remotely operated vehicle," *IEEE Trans. Control Syst. Technol.*, vol. 19, no. 5, pp. 1036–1046, Sep. 2011.
- [19] G. Fagogenis, V. De Carolis, and D. M. Lane, "Online fault detection and model adaptation for underwater vehicles in the case of thruster failures," in *Proc. IEEE Int. Conf. Robot. Automat. (ICRA)*, May 2016, pp. 2625–2630.
- [20] N. Wang, X. Pan, and S.-F. Su, "Finite-time fault-tolerant trajectory tracking control of an autonomous surface vehicle," *J. Franklin Inst.*, vol. 357, no. 16, pp. 11114–11135, Nov. 2020. [Online]. Available: <https://www.sciencedirect.com/science/article/pii/S0016003219303461>
- [21] C. Hacizade and S. Y. Vural, "Active fault tolerant lateral control against actuator faults applied to AUV dynamics," in *Proc. 4th Conf. Control Fault Tolerant Syst. (SysTol)*, Sep. 2019, pp. 153–158.
- [22] A. Inzartsev, A. Pavin, A. Kleschev, V. Gribova, and G. Eliseenko, "Application of artificial intelligence techniques for fault diagnostics of autonomous underwater vehicles," in *Proc. OCEANS MTS/IEEE Monterey*, Sep. 2016, pp. 1–6.
- [23] X. Liu, M. Zhang, and F. Yao, "Adaptive fault tolerant control and thruster fault reconstruction for autonomous underwater vehicle," *Ocean Eng.*, vol. 155, pp. 10–23, May 2018. [Online]. Available: <http://www.sciencedirect.com/science/article/pii/S0029801818301471>
- [24] Y. Wang, B. Jiang, Z. Wu, S. Xie, and Y. Peng, "Adaptive sliding mode fault-tolerant fuzzy tracking control with application to unmanned marine vehicles," *IEEE Trans. Syst., Man, Cybern. Syst.*, vol. 51, no. 11, pp. 1–10, Nov. 2020.
- [25] L.-Y. Hao, H. Zhang, T.-S. Li, B. Lin, and C. L. P. Chen, "Fault tolerant control for dynamic positioning of unmanned marine vehicles based on T-S fuzzy model with unknown membership functions," *IEEE Trans. Veh. Technol.*, vol. 70, no. 1, pp. 146–157, Jan. 2021.
- [26] Z. Zhou, M. Zhong, and Y. Wang, "Fault diagnosis observer and fault-tolerant control design for unmanned surface vehicles in network environments," *IEEE Access*, vol. 7, pp. 173694–173702, 2019.
- [27] L.-Y. Hao, H. Zhang, H. Li, and T.-S. Li, "Sliding mode fault-tolerant control for unmanned marine vehicles with signal quantization and time-delay," *Ocean Eng.*, vol. 215, Nov. 2020, Art. no. 107882. [Online]. Available: <https://www.sciencedirect.com/science/article/pii/S0029801820308465>
- [28] L.-Y. Hao, Y.-Q. Zhang, and H. Li, "Fault-tolerant control via integral sliding mode output feedback for unmanned marine vehicles," *Appl. Math. Comput.*, vol. 401, Jul. 2021, Art. no. 126078. [Online]. Available: <https://www.sciencedirect.com/science/article/pii/S0096300321001260>
- [29] A. A. Amin and K. M. Hasan, "A review of fault tolerant control systems: Advancements and applications," *Measurement*, vol. 143, pp. 58–68, Sep. 2019. [Online]. Available: <https://www.sciencedirect.com/science/article/pii/S0263224119304099>
- [30] D. Chaos, D. Moreno-Salinas, R. Mu noz-Mansilla, and J. Aranda, "Non-linear control for trajectory tracking of a nonholonomic RC-hovercraft with discrete inputs," *Math. Problems Eng.*, vol. 2013, Jan. 2013, Art. no. 589267.
- [31] D. Moreno-Salinas, D. Chaos, J. M. de la Cruz, and J. Aranda, "Identification of a surface marine vessel using LS-SVM," *J. Appl. Math.*, vol. 2013, Apr. 2013, Art. no. 803548.
- [32] D. Moreno-Salinas, D. Chaos, E. Besada-Portas, J. A. López-Orozco, J. M. de la Cruz, and J. Aranda, "Semophysical modelling of the nonlinear dynamics of a surface craft with LS-SVM," *Math. Problems Eng.*, vol. 2013, Oct. 2013, Art. no. 890120.
- [33] D. Moreno-Salinas, R. Moreno, A. Pereira, J. Aranda, and J. M. de la Cruz, "Modelling of a surface marine vehicle with kernel ridge regression confidence machine," *Appl. Soft Comput.*, vol. 76, pp. 237–250, Mar. 2019. [Online]. Available: <http://www.sciencedirect.com/science/article/pii/S1568494618306847>
- [34] R. Moreno, D. Moreno-Salinas, and J. Aranda, "Black-box marine vehicle identification with regression techniques for random manoeuvres," *Electronics*, vol. 8, no. 5, p. 492, Apr. 2019.
- [35] *Nomenclature for Treating the Motion of a Sumerged Body Through a Fluid*, SNAME, Soc. Naval Architects Marine Eng., New York, NY, USA, 1950.
- [36] T. I. Fossen, *Marine Control Systems: Guidance, Navigation and Control of Ships, Rigs and Underwater Vehicles*. Trondheim, Norway: Marine Cybernetics AS, 2002.
- [37] A. P. Aguiar and A. M. Pascoal, "Regulation of a nonholonomic autonomous underwater vehicle with parametric modeling uncertainty using Lyapunov functions," in *Proc. 40th IEEE Conf. Decis. Control*, Dec. 2001, pp. 4178–4183.
- [38] H. K. Khalil, *Nonlinear Systems*, 3rd ed. Upper Saddle River, NJ, USA: Prentice-Hall, 2002.
- [39] T. M. Apostol, *Mathematical Analysis—A Modern Approach to Advanced Calculus*. Reading, MA, USA: Addison-Wesley, 1957.
- [40] M. Spivak, *Calculus*, 2nd ed. New York, NY, USA: W. A. Benjamin, 1992.



DICTINO CHAOS received the B.D. degree in physics from the Complutense University of Madrid, in 2004, and the Ph.D. degree in computer engineering and automatic control from UNED, in 2010. He is currently an Associate Professor with the Department of Computer Science and Automatic Control, UNED. His research interests include nonlinear control, tracking, point stabilization, and path following of under-actuated vehicles, the stability of switched systems, machine vision, and robotics. He was awarded with the Special Prize for the Best Ph.D. Thesis at UNED.



DAVID MORENO-SALINAS received the degree in industrial electronics engineering and the degree in automatic control and electronics engineering from the University of Cordoba, in 2003 and 2006, respectively, and the Ph.D. degree in computer science from the National University Distance Education (UNED), in 2013. He worked for the Agency of Research and Development of the regional government of Andalusia, from 2006 to 2007. Since 2007, he has been with the Department of Computer Science and Automatic Control, since 2010, he has been an Assistant Professor, and since 2018, he has been an Associate Professor. His scientific interests include estimation, positioning, sensor networks, modeling and simulation, and control and robotics.



JOAQUÍN ARANDA received the Licentiate degree from the Complutense University of Madrid, in 1983, and the Ph.D. degree from the Distance University of Spain (UNED), in 1989. He worked as a Teaching Assistant with the Computer Science and Automatic Control Department, Complutense University of Madrid. Since 1988, he has been with the Computer Science and Automatic Control Department, UNED, where he is currently a Full Professor. He was the Deputy Director of the University School of Computer Science, UNED, from 1997 to 2001, and the Director of the Computer Science High School, from 2001 to 2005. He has been leading the research group about industrial computing, since 1997. He was the Head of the Computer Science and Automatic Control Department, UNED, from 2007 to 2014. He is the author or the coauthor of more than 120 publications, including books chapters, articles in journals, and conference proceedings. His scientific interests include control engineering field: controller design, robust control, computer control, modeling and simulation, and application of control and simulation to high speed craft, marine systems, airplanes, and robotics.

• • •